THE UNIVERSITY of EDINBURGH

Edinburgh Research Explorer

# Characterizing Concrete Surface Notch using Rayleigh Wave Phase Velocity and Wavelet Parametric Analyses

**Citation for published version:**
Lee, FW, Chai, HK & Lim, KS 2016, 'Characterizing Concrete Surface Notch using Rayleigh Wave Phase Velocity and Wavelet Parametric Analyses', *Construction and Building Materials*.
https://doi.org/10.1016/j.conbuildmat.2016.08.145

**Digital Object Identifier (DOI):**
10.1016/j.conbuildmat.2016.08.145

**Link:**
Link to publication record in Edinburgh Research Explorer

**Document Version:**
Peer reviewed version

**Published In:**
Construction and Building Materials

**General rights**
Copyright for the publications made accessible via the Edinburgh Research Explorer is retained by the author(s) and / or other copyright owners and it is a condition of accessing these publications that users recognise and abide by the legal requirements associated with these rights.

**Take down policy**
The University of Edinburgh has made every reasonable effort to ensure that Edinburgh Research Explorer content complies with UK legislation. If you believe that the public display of this file breaches copyright please contact openaccess@ed.ac.uk providing details, and we will remove access to the work immediately and investigate your claim.

OPEN ACCESS

Download date: 11. May. 2020

*Manuscript
Click here to view linked References

# Characterizing Concrete Surface Notch using Rayleigh Wave Phase Velocity and Wavelet Parametric Analyses

**Foo Wei Lee[(1)], Hwa Kian Chai*[(2)], Kok Sing Lim[(3)]**

(1) Department of Civil Engineering, University of Malaya, Kuala Lumpur, Malaysia.

(2) School of Engineering, The University of Edinburgh, Edinburgh, Scotland.

(3) Photonics Research Centre, University of Malaya, Kuala Lumpur, Malaysia.

**Abstract:** A multichannel Rayleigh wave (R-wave) measurement technique is proposed for evaluating concrete surface notches with different orientations. In this study, numerical simulations were first conducted to examine the propagation of R-waves in steel-reinforced concrete comprising of surface notch inclining at 30°, 90° and 150° against the horizontal plane. The change of R-wave amplitude was obtained through analysis by wavelet transform (WT) and fast Fourier transform (FFT) for determining theirs correlations with the notch depth-to-wavelength ratio. Experimental measurements on concrete samples were then carried out to validate the proposed technique and its performance, particularly for cases where notch depth is greater than R-wave wavelength. Good agreement was found between the experimental results and the numerical calculations, offering good possibility for using R-waves to assess vertical and inclined surface notches in reinforced concrete with the proposed technique for R-waves acquisition and analysis.

**Keywords:** reinforced-concrete; surface notch; Rayleigh wave; wavelet transform; phase velocity; excitation frequency

Corresponding author.
Postal address: School of Engineering, The University of Edinburgh, Sanderson Building, Robert Stevenson Road, The King's Buildings, Edinburgh, Scotland.
Email address: hwakian.chai@gmail.com

# 1. Introduction

Concrete structures deteriorate over time as a consequence of pro-longed exposure to various environmental factors for instance the mechanical loading, extreme weather and other forces of nature. Surface cracking is one of the most common defects found in concrete structures. It is the result of the combined effect of drying shrinkage, thermal variation, restraint (external or internal) to shortening, subgrade settlement or mechanical actions like fatigue and overloading [1, 2]. Strategic monitoring and assessment on the condition and health of these structures are needed to prevent further deterioration in the structures which will lead to fracture or even collapse due to the loss of structural integrity. Non-destructive testing (NDT) is a wide group of non-invasive analysis methods which is able to provide information about the internal condition of concrete. Elastic waves methods are amongst some of the popular NDT techniques used for detecting defects and damages in concrete structures. Surface Rayleigh wave (R-wave) that propagates along the surface of the structure had been used in the study and evaluation of the integrity of concrete structures. For example, strength gain evaluation of early-age concrete exposed to different curing conditions [3]; investigation of the relationship between R-wave velocity and porosity in dry and fully saturated mortar and porosity estimation in concrete cover from ultrasonic measurements [4]; aggregate segregation detection in asphaltic concrete based on the phase velocity and attenuation of R-wave by wedge generation technique along with an air-coupled receiving transducer with a finite-size aperture [5]; examination of concrete blocks, including subsurface cracks with different depths by ultrasound method [6]; honeycomb inspection in early-age concrete by ultrasonic surface wave [7]; application of Second Harmonic Generation (SHG) in R-waves to quantify microstructural changes and microcracks in mortar and concrete [8]; feasibility study of defects detection inside reinforced concrete (RC) structures by using elastic-wave based multi-directional Synthetic Aperture Focusing Technique (SAFT) [9].

Many efforts make use of characteristics of R-waves such as scattering and attenuation in the application of surface cracks detection and estimation. For example, non-contact, air-coupled surface wave transmission and the effects of sensor locations were investigated for partially or fully closed surface breaking crack by [10-14]. In addition, a two sensor-array methodology was implemented by [15] for effective in-place crack depth estimation based on the study of concrete specimens with vertical slits of different depths. Apart from that, Rayleigh wave dispersion and energy dissipation were analyzed to determine the locations and the depths of surface cracks in concrete beams [16]. Besides, surface crack depth estimation and the evaluation of repair effect for deteriorated concrete piers were analytically and experimentally investigated using Rayleigh waves by [17-20]. Despite these, most of the studies have been associated with estimating concrete cracks that are relatively shallow in depth and the propagation of R-waves in concrete containing an inclined crack has not been investigated in detail to the author's best knowledge. In a most recent effort, we performed multi-channel measurements of R-waves on concrete specimens with surface defects [21, 22]. With the previous numerical and experimental findings serving as the fundamental and knowing the potential of R-waves as an effective means for assessing concrete cracks [23, 24], the aim of this study is to establish an in-depth understanding and quantitative relations useful for characterizing the surface notch, e.g. depth and degree of inclination. A series of simulations for wave motions to examine the behavior of R-waves of varying excitation frequencies towards different depths and degree of inclinations of surface notch were carried out. The outcome of this study is considered to provide further insights on identifying the critical parameters (WT and phase velocity) for quantification of correlations that lead towards establishing a reliable assessment method for concrete structures with similar defective conditions. The simulated R-waves results for different notch depths and inclination angles were then verified through experimental measurements.

## 2. Numerical Simulations

The simulations were conducted by employing commercial software [25] that solves two dimensional (2D) elastic wave propagation problems by temporal acoustic interrogations based on the finite difference method in the plain strain case. The fundamental equation governing the two-dimensional propagation of stress waves in a perfectly elastic medium, ignoring viscous losses is as follows [25]:

$$\rho \frac{\partial^2 u}{\partial t^2} = \mu \nabla^2 u + (\lambda + \mu) \nabla (\nabla \bullet u) \tag{1}$$

where $u = u\,(x, y, t)$is the time-varying displacement vector, $\rho$ is material density, $\lambda$ is first Lame constant, $\mu$ is second Lame constant, $\nabla$ is the gradient of operator, $\nabla \bullet$ is the divergence operator, $\partial$ is the partial differential operator, *t* is the time. Eq. (1) is solved at discrete points with respect to the boundary conditions of the model, which include the input source that has predefined time-dependent displacements at a given location and a set of initial conditions, while wave propagation in each distinct homogeneous phase is solved according to Eq. (1) as well [26, 27].

A two dimensional steel reinforced concrete model with a dimension of 500 mm (width) × 300 mm (depth) was proposed (see Figure 1). All materials were considered elastic without viscosity components. The mechanical properties of the concrete and steel reinforcement were configured as uniform throughout the whole study and produced longitudinal wave velocities of approximately 4300 m/s and 6099 m/s, for concrete and steel reinforcement, respectively. The source of wave was configured as excitations by impacts (point source), which was located on the top surface and produced a full cycle elastic wave with different range of frequencies in order to estimate the effect of the different wavelengths. In the simulation, three sensors were placed on the left and right side of the inclined surface notch, respectively with spacing of 40 mm. The distance between the source and nearest sensor S1 was set to 170 mm to avoid significant the near and far field effects. From the simulation, the influence of notch on waveform distortion, reduction of amplitude and pulse velocity was assessed. For time sampling, the step was 0.0962 $\mu$s while the basic period of the highest frequency (150 kHz) was 6.67 $\mu$s, implying that a typical cycle was represented by almost 70 points, more than 10–20 points which are considered adequate. Table 1 tabulates the elastic properties of simulation model, which were obtained and calculated from laboratory testing and wave measurement of concrete specimen. The material and geometry of concrete medium set as uniform throughout the simulation work. In addition, the parameters of investigation such as angle of inclination, vertical depth, and frequency of excitation are provided in Table 2.

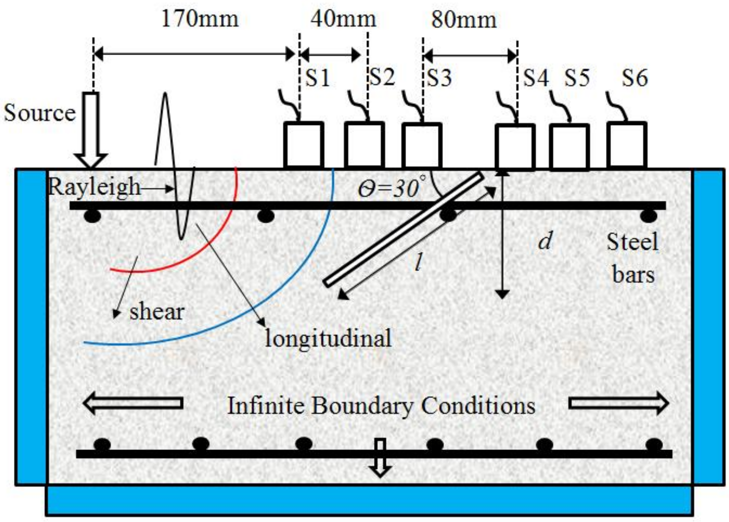


**Figure 1.** Wave motion simulation model.

**Table 1.** Properties of steel reinforced concrete model

| PARAMETER | Concrete Model | Reinforcing Steel |
|---|---|---|
| Lambda, $\lambda_m$ | 15457 MPa | 12482 MPa |
| Mu, $\mu_m$ | 14600 MPa | 83590 MPa |
| Density, $\rho_m$ | 2313 kg/m$^3$ | 7850 kg/m$^3$ |
| P-wave velocity, $V_P$ | 4394.92 m/s | 6099.28 m/s |
| R-wave velocity, $V_R$ | 2311.96 m/s | 3219.95 m/s |
| Wavelength of R-wave, $\lambda_R$ | 2.31 mm | 3.22 mm |

**Table 2.** Characteristics of simulated notches

| Types of defect | Depth, *d* (mm) | Length, *l* (mm) | Degree of inclination $\theta$, (°) to the horizontal plane | Frequency of wave, *f* (kHz) |
|---|---|---|---|---|
| Surface notch | 15, 30, 45, 60, 75, 90, 120, 150 | 30 to 150 at 30 mm increment | 30, 90, 150 | 10, 20, 30, 40, 50, 60, 80, 100, 150 |

## 3. Signal Processing and Waveform Analysis

In this study, matched filtering of center of energy (MFCE) technique was employed in raw data signal processing. It is understood that R-wave carries a higher amount of energy than body waves. The developed MFCE technique is useful for extracting R-wave component from the recorded waveforms, based on identification of wave amplitudes corresponding to R-waves. The MFCE technique could identify the location of the center of energy for R-wave and "zero pad" the amplitudes of other waves while keeping the one related to the arrival of R-wave, which was usually signified by a large increase in both the positive and negative phase in the waveform. After that, matched filtering on each processed signal was executed with respect to the processed signal obtained from the first sensor. The details of the technique can be found in [23]. The windowed signals (R-waves) after the MFCE process were further analyzed by WT and FFT techniques. FFT was performed on the processed data and from the resulting frequency response, phase difference between first sensor and following sensors was calculated. Phase velocity component of R-waves for a particular frequency was the obtained using the following equation [28, 29]:

$$V_p = \lambda f = \frac{2\pi f \, \Delta x}{\Delta\varphi} \tag{2}$$

where $V_p$ is phase velocity, $\pi$ is phi, $\lambda$ is wavelength, $f$ is corresponding frequency, $\Delta x$ is the distance between sensors and $\Delta\varphi$ is phase difference which defined as the difference between unwrapped angle for processed signals detected by each sensor. In addition, the continuous wavelet transform (CWT) based on the Gabor wavelets, which has been demonstrated to be very useful as a time-frequency analysis tool of wave signals in SHM [30-34], is used to calculate a dispersion-invariant maximum point in the processed signal. Theoretically, the CWT is defined as [35]:

$$F_\Psi(a,b) = \frac{1}{\sqrt{a}} \int_{-\infty}^{\infty} f(t)\, \Psi(\frac{t-b}{a})dt \tag{3}$$

where $\Psi(t)$ is a mother wavelet with finite energy, $a$ is a scale parameter, $F_\Psi(a,b)$ is a wavelet coefficient for a given time domain signal f(t). Any mother wavelet can be used for a wavelet transform, which is the major advantage of the wavelet transform. The mother wavelet used in study was Gabor wavelet based on the Gaussian function and its Fourier transform are given as [36] due to the similarity in shape to the raw waveforms and could lead to a more consistent results:

$$\Psi(t) = \frac{1}{\sqrt[4]{\pi}} \sqrt{\frac{\omega_p}{\gamma}}\, exp\left[-\frac{t^2}{2}\left(\frac{\omega_p}{\gamma}\right)^2 + i\omega_p t\right] \tag{4}$$

$$\widehat{\Psi}(\omega) = \frac{\sqrt{2\pi}}{\sqrt[4]{\pi}} \sqrt{\frac{\omega_p}{\gamma}}\, exp\left[-\frac{t^2}{2}\left(\frac{\omega_p}{\gamma}\right)^2 (\omega - \omega_p)^2\right] \tag{5}$$

where, $\omega_p$ is the center frequency, $\omega = 2\pi$, $\gamma$ is a constant taken as $\gamma = \pi(2/\ln 2)^{1/2}$. The identified frequency (corresponding to peak coefficient intensity) from sensor S1 was used to correlate with the rest of wavelet transforms. Generally, the information about standard time and frequency content and wavelet transform coefficient can be obtained from the algorithm. Meanwhile, the distribution of wavelet transform coefficient is shown in the form of a contour plot. Since the transform distributes the energy of a wave in time and frequency, hence it is possible to identify the occurrence of particular frequency content at a certain time.

## 4. Materials, sensors and excitation

Four steel reinforced concrete block specimens of 300 × 300 × 500 mm were cast and the experimental set-up as shown in Figure 2. Among the specimens, one served as the control sample, while the rest consisted of an artificial notch inclining at 30°, 90° and 150°. A triangular shaped polystyrene foam board was employed to represent surface notch that has different "notch depths" along the transverse direction of the specimen. For experiment measurement, piezoelectric accelerometers (by ICP®) with frequency range of 0.005 kHz to 60 kHz were used. As illustrated in Figure 2, six accelerometers were placed on the top surface of the specimen, in an arrangement similar to the one adopted in the simulation. Elastic wave excitations were made by dropping steel balls onto the concrete surface at 170 mm away from the trigger sensor S1. Throughout the experiment, steel ball impacts were implemented by the same operator to minimize inconsistencies in the generation of stress waves. Steel balls with different sizes were used for the purpose of generation of R-waves with different dominant frequencies to investigate the relations between wavelength, notch depth, angle of inclination and change in amplitude as well as the velocity. It was known that as the diameter of the steel ball becomes smaller, the corresponding dominant frequency becomes higher [37]. In this study, wave excitations were conducted from both sides for the

Control specimen and the one with vertical notch to minimize the geometrical effect. On the other hand, for specimens with 30° and 150° inclined notches, excitation was carried out on concrete surface at both sides of the notch and the waveforms were stacked to enhance signal consistency and the sound-to-noise ratio. To ensure good coupling between sensor and concrete, electron wax was used for mounting the sensors.

A waveform acquisition system (PXIe-4492 by National Instruments Co.) was used to conduct measurement and record waveform data with an interval of 5 μs for a period of 0.02 seconds. The elastic waves consist of longitudinal, shear (spreading into the specimen with a spherical wavefront) and R-waves (confined near the surface (see Figure. 1)). The accelerometers can record the strongest Rayleigh mode and also the initial part of longitudinal wave which is the fastest type and arrives first at detection point.

**Figure 2.** Photograph of accelerometer sensors arranged on the upper side of concrete specimen.

## 5. Results

### *5. Waveforms and Signal Processing*

Figures 3 (a) and (b) show typical waveforms obtained from simulating models without notch, which were generated by excitation frequencies of 10 and 150 kHz. The strong burst in the waveform belongs to the Rayleigh mode was observed, which follows the weak initial arrival of the P-wave, especially for higher excitation frequencies due to its lower velocity and slowest types. Simulated waveforms of various notched concrete models acquired from same excitation frequencies are also shown in Figures 3 (c) to (n). Distorted waveforms recorded by sensors S4, S5 and S6, located on the side after the notch indicated an abrupt decrease in amplitude (waveforms were magnified by a factor of 8 in Figures 3 (f), (j) and (n)) as compared to those obtained from the sensors of sound concrete model or the ones located before the notch (S1, S2 and S3), which are visible. A portion of the waves was reflected back when they impinged on the free surface of a notch, while the other portion passed through below the notch. The waves were then diffracted and scattered when they impinged on the tip of the notch [38]. In addition, the arrival of R-waves has obviously been delayed, especially in the deeper notch cases (150 mm). This reveals that less energy is transmitted through the notch for a longer pathway before reaching the corresponding sensors. Clearly, the depth of the notch has tremendous influence on the wave amplitude and the transit time of the signal as recorded by sensors after the notch.

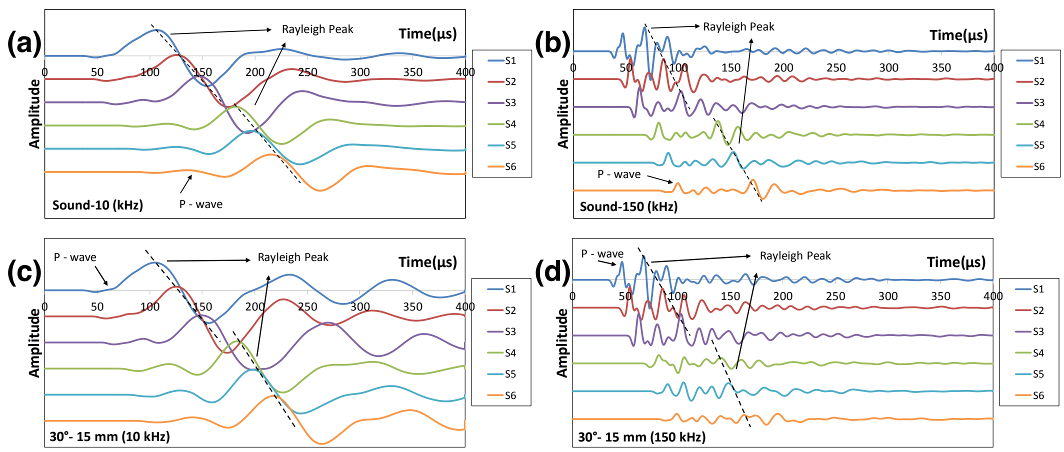

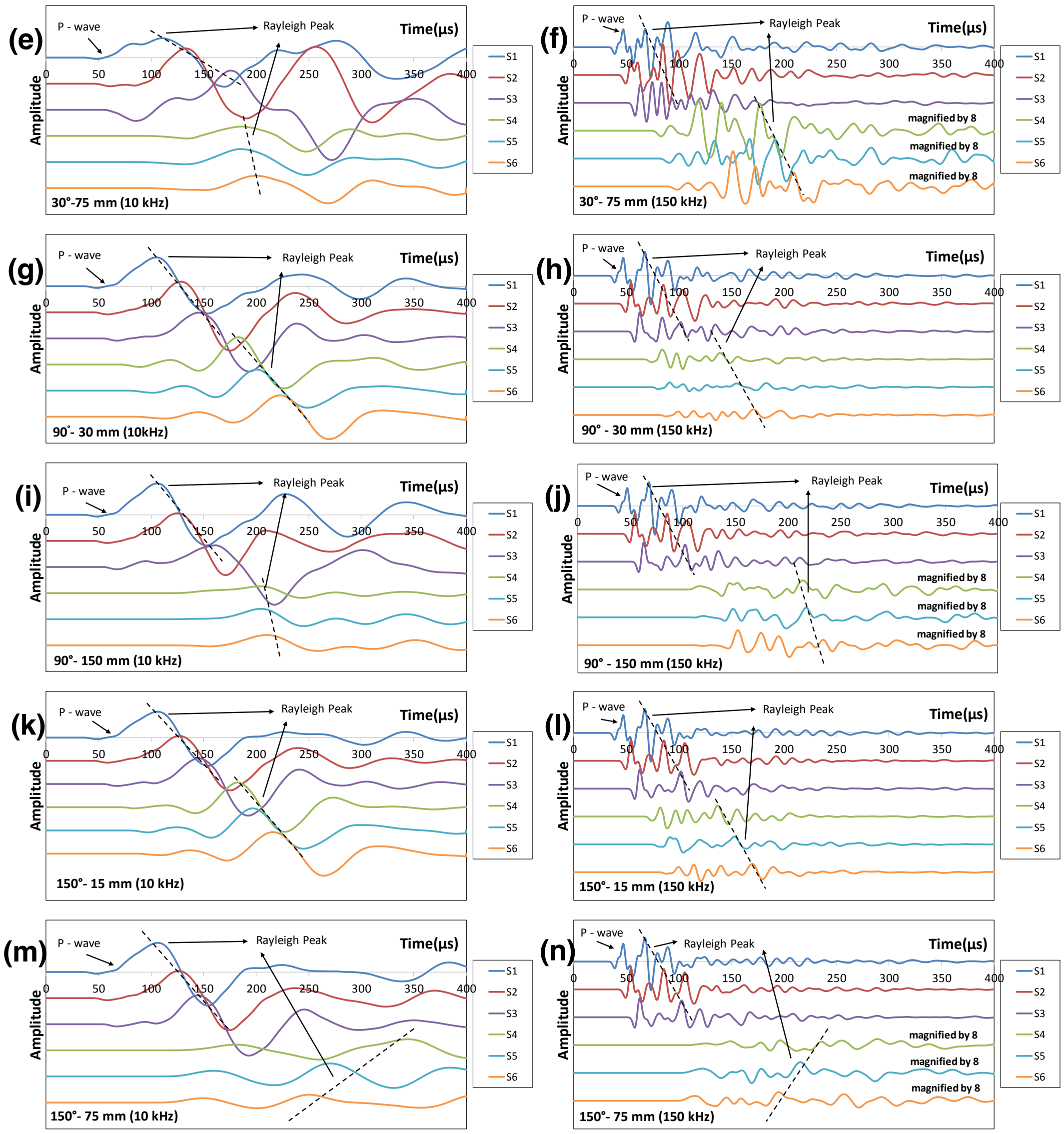


**Figure 3.** Simulated waveforms collected from steel reinforced concrete model for sound concrete mode using (a) 10 kHz and (b) 150 kHz excitations; 15 mm 30° inclined notch using (c) 10 kHz and (d) 150 kHz excitations; for 75 mm 30° inclined notch using (e) 10 kHz and (f) 150 kHz excitations; for 30 mm 90° vertical notch using (g) 10 kHz and (h) 150 kHz excitations; for 150 mm 90° vertical notch using (i) 10 kHz and (j) 150 kHz excitations; for 15 mm 150° inclined notch using (k) 10 kHz and (l) 150 kHz excitations; for 75 mm 150° inclined notch using (m) 10 kHz and (n) 150 kHz excitations

Examples of raw and MFCE processed waveforms acquired from sensor S4 were presented in Figure 4. The R-wave peak is indicated by red circle, while the P-wave is marked by green cross to distinguish the arrivals of P- and R-waves. The window was applied around the center of energy of R-wave, while the rest of the waveform was zero-padded as can be seen in Figure 4. In order to comprise one full cycle of elastic wave components, the length of windows adopted in this study is set to at least 1.5 times greater than its excitation wavelength. The processed waveform resulted in a more clear-cut isolated component, indicating a characteristic peak arrival belonging to the R-wave. Moreover, the processed waveform was found to yield peak frequency very similar to the frequency of excitation, indicating that the this frequency could be regarded as the characteristic frequency of the R-waves generated.

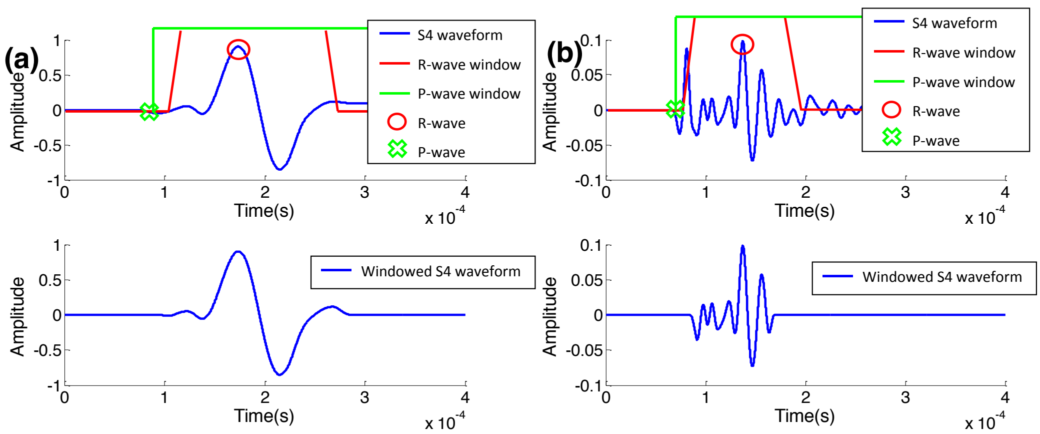


**Figure 4.** Processing of waveforms using proposed matched filtering algorithm from sensor S4 for sound steel reinforced concrete model using (a) 10 kHz and (b) 150 kHz excitations

Figure 5 shows the processed waveforms and the respective R-wave peak matched positions based on MFCE technique for sound and various notches concrete models with excitation frequencies of 10 kHz and 150 kHz, respectively. The variations of amplitude and the delayed of R-wave peaks were almost identical and comparable to the raw data as shown in Figure 3, showing the performance of the proposed MFCE algorithm in determination and extraction of R-wave components from raw waveform data.

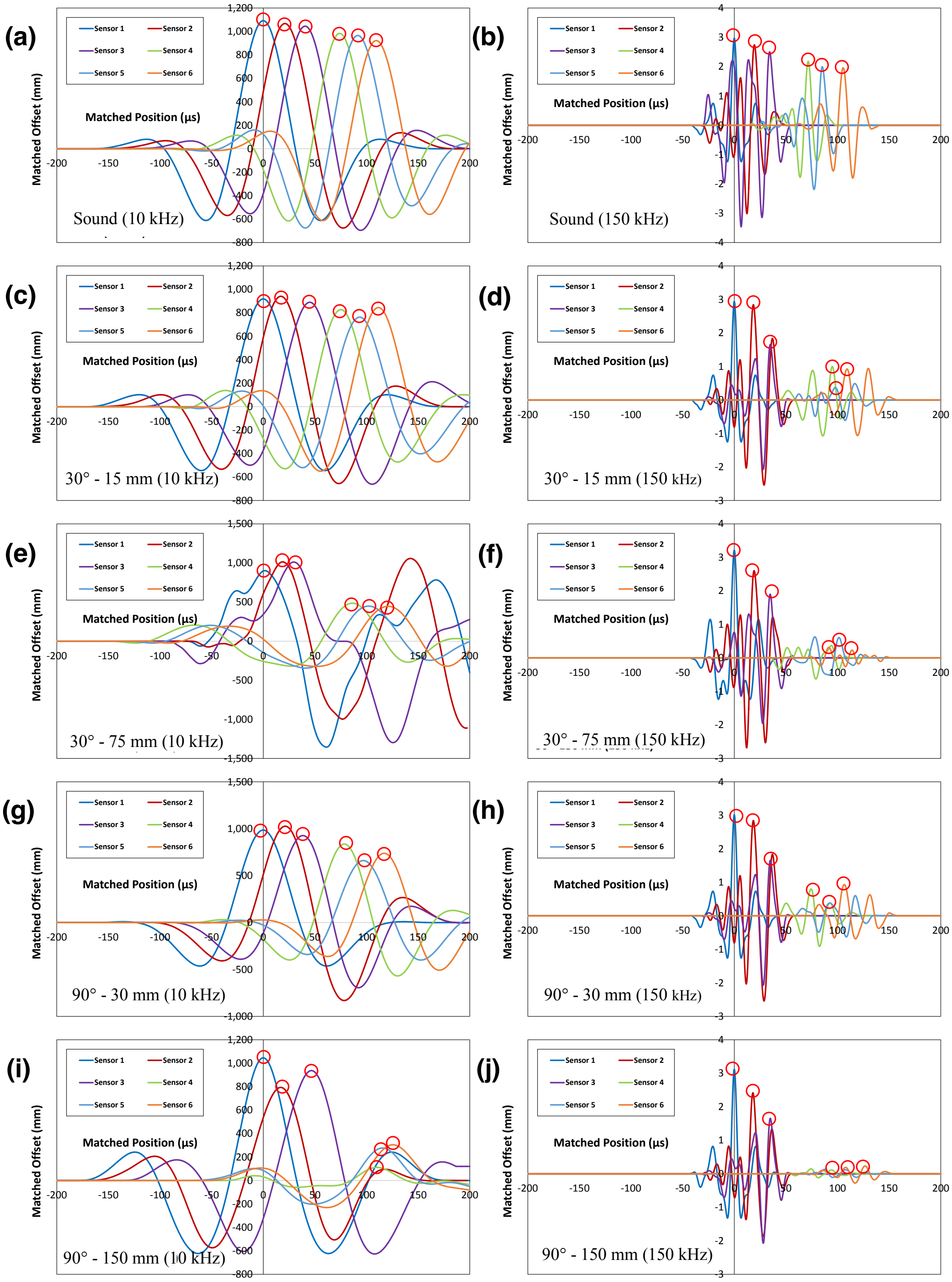

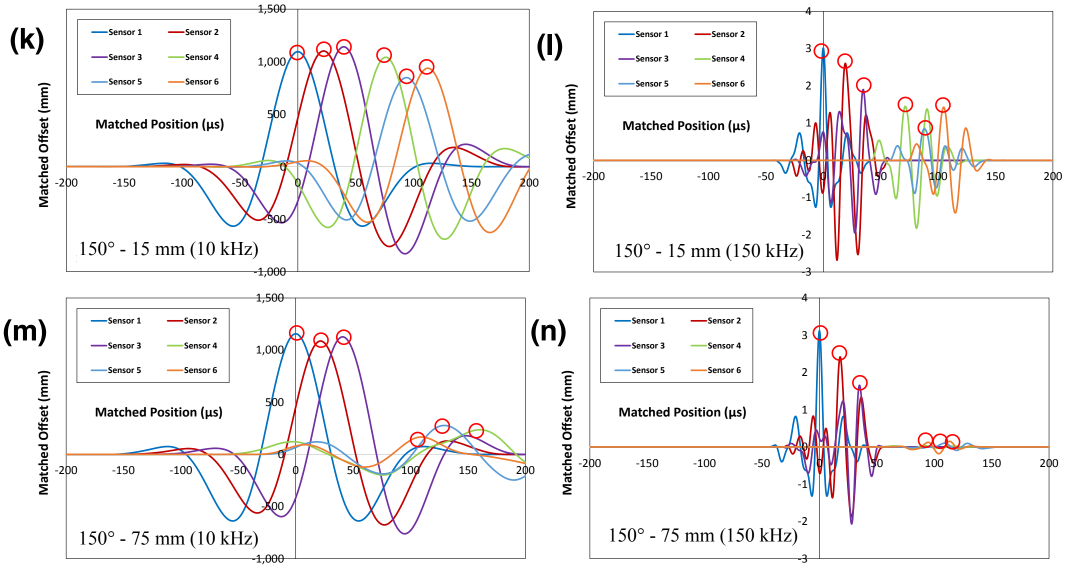


**Figure 5.** Processed waveforms and the respective final R-wave peak matched positions based on MFCE method for sound concrete model using (a) 10 kHz and (b) 150 kHz excitations; for 15 mm 30° inclined notch using (c) 10 kHz and (d) 150 kHz excitations; for 75 mm 30° inclined notch using (e) 10 kHz and (f) 150 kHz excitations; for 30 mm 90° vertical notch using (g) 10 kHz and (h) 150 kHz excitations; for 150 mm 90° vertical notch using (i) 10 kHz and (j) 150 kHz excitations; for 15 mm 150° inclined notch using (k) 10 kHz and (l) 150 kHz excitations; for 75 mm 150° inclined notch using (m) 10 kHz and (n) 150 kHz excitations

Dispersion curve was utilized to explain the change of phase velocity of R-waves against the surface notch within the effective frequency bandwidth of excitation. The effective frequency bandwidth was determined based on the frequency domain function of the received signals and this bandwidth of frequencies containing most of the signal energy, which indicating a characteristic peak frequency belonging to the propagating R-waves by FFT and by Eq.2. Examples of averaged dispersion curve of each sensor (S1)-sensor combination for sound and various surface notched concrete model cases are depicted in

Figure 6 for the data obtained from 10 kHz and 150 kHz excitations, respectively. The dispersion curves for the sound concrete model were almost consistent throughout the bandwidth under consideration, giving an averaged value of 2295 m/s at 10 kHz and 2398 m/s at 150 kHz frequencies, which was very close to that calculated by considering the arrival time of Rayleigh peaks. In contrary, the measured averaged phase velocity of model with a surface notch depth of 150 mm was only 1571 m/s at 10 kHz and 1236 m/s at 150 kHz, which were 31.5 % and 48.4 %, respectively, lower than that of the sound concrete model. Further, it can be seen that the respective dispersion curves have been translated to lower values and were less consistent throughout the bandwidth under consideration. The overall calculated dispersion curves are clearly delayed because of the presence of surface notch, and the curve shape was changed for the steel reinforced concrete models. It is worth to note that the frequency at source shows symmetric, Gaussian-like curve but frequency attenuation is likely to happen after propagating concrete. Therefore, the FFT for sensors may no longer be symmetric. The change of "intensity of frequency" (amplitude of each frequency component) across the indicated bandwidth could result in asymmetric distribution of phase velocity. The recorded phase velocities were used to calculate phase velocity index using equation:

$$PVI = \frac{\sum_{j=2}^{6} PV_{n,1\sim j} /6}{\sum_{j=2}^{6} PV_{s,1\sim j} /6} \quad (6)$$

where $\sum_{j=2}^{6} PV_{n,1\sim j} /6$ and $\sum_{j=2}^{6} PV_{s,1\sim j} /6$ are average of R-wave phase velocities from Sensor S1 to the other sensors, respectively, for model with notch and the sound model, respectively.

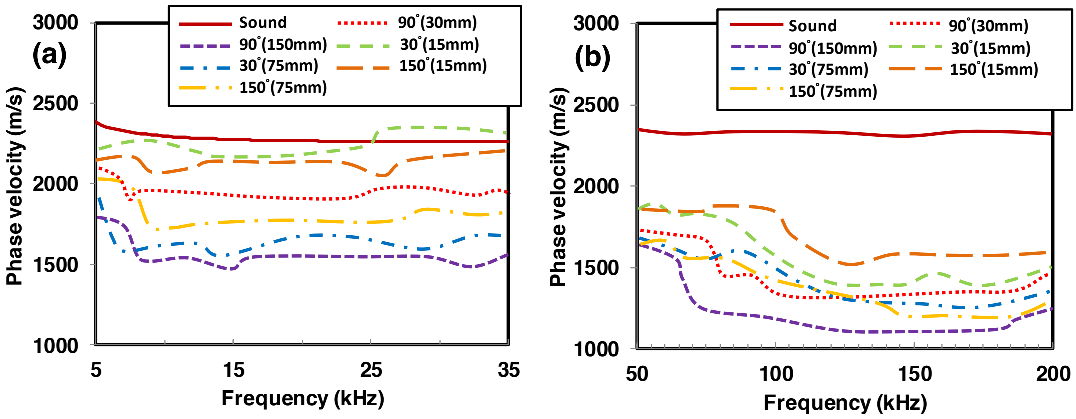


**Figure 6.** Dispersion curve computed for sound and various surface notched concrete models using (a) 10 kHz and (b) 150 kHz excitations

Figure 7 shows the examples of 2D distribution of wavelet transform for 10 kHz and 150 kHz excitations as well as for steel reinforced concrete models at sensor S4 (sensor after the surface notch). The wavelet transform diagram shows the magnitudes of wavelet transform auto scaled in rainbow colors, which lower magnitudes correspond to pink while peak magnitudes correspond to red. The peak energy intensity or the arrival of the wave peak at each frequency component can be easily obtained. The identified peak intensity which is corresponding to the respective R-wave amplitude was recorded for further analysis and interpretation using:

$$WTI = \frac{\prod_{j=4}^{6} WT_{n,j} \, / \prod_{i=1}^{3} WT_{n,i}}{\prod_{j=4}^{6} WT_{s,j} \, / \prod_{i=1}^{3} WT_{s,i}} \tag{7}$$

where $WT_n$ is R-wave WT coefficient in model with notch, $WT_s$ is R-wave WT coefficient in sound model. The magnitudes of the wavelet transform (peak energy intensity) obtained from sensor S4 were significantly lower for both the 150 mm depth vertical and 75 mm inclined notch cases as compared to the one obtained from the sound reinforced concrete model. In addition, delayed of peak energy intensity was noticed as well, in particular for the deeper notch depth cases.

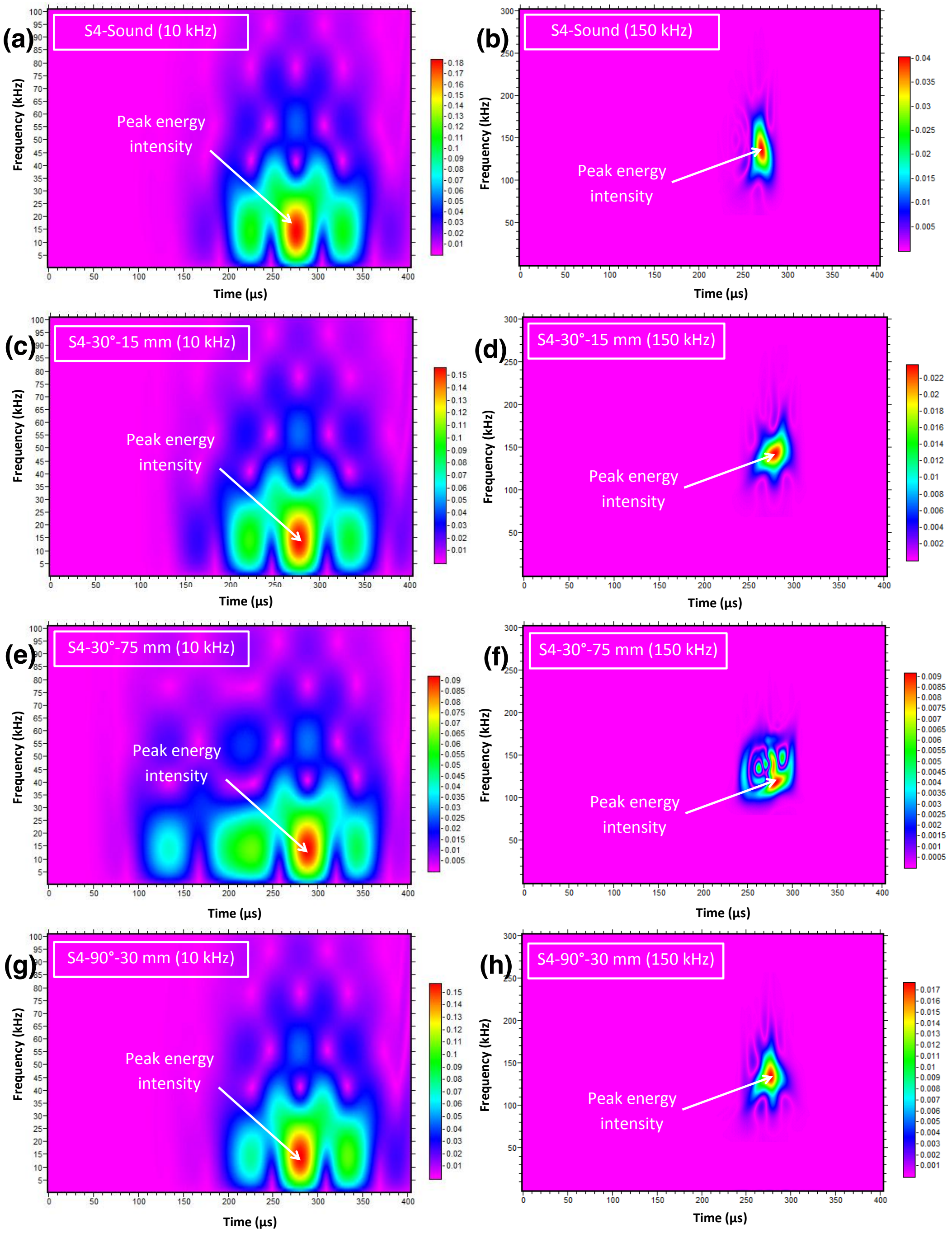
(a)
S4-Sound (10 kHz)
Peak energy intensity
Frequency (kHz)
Time (µs)
(b)
S4-Sound (150 kHz)
Peak energy intensity
Frequency (kHz)
Time (µs)
(c)
S4-30°-15 mm (10 kHz)
Peak energy intensity
Frequency (kHz)
Time (µs)
(d)
S4-30°-15 mm (150 kHz)
Peak energy intensity
Frequency (kHz)
Time (µs)
(e)
S4-30°-75 mm (10 kHz)
Peak energy intensity
Frequency (kHz)
Time (µs)
(f)
S4-30°-75 mm (150 kHz)
Peak energy intensity
Frequency (kHz)
Time (µs)
(g)
S4-90°-30 mm (10 kHz)
Peak energy intensity
Frequency (kHz)
Time (µs)
(h)
S4-90°-30 mm (150 kHz)
Peak energy intensity
Frequency (kHz)
Time (µs)

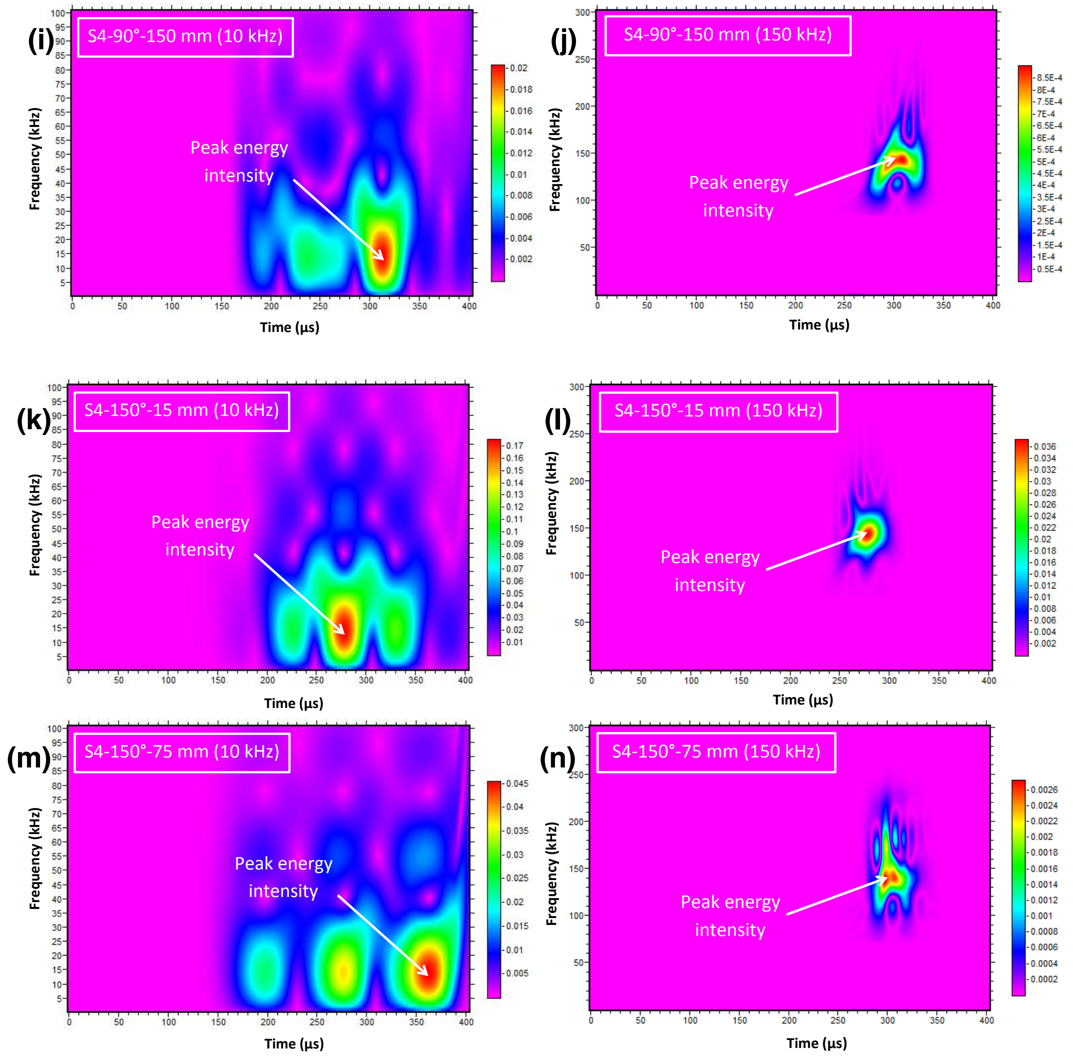


**Figure 7.** 2D wavelet transform contour diagram at the fourth sensors (S4) for steel reinforced concrete model using (a) 10 kHz and (b) 150 kHz; for 15 mm 30° inclined notch model using (c) 10 kHz and (d) 150 kHz excitations; for 75 mm 30° inclined notch model using (e) 10 kHz and (f) 150 kHz excitations; or 30 mm 90° vertical notch model using (g) 10 kHz and (h) 150 kHz excitations; for 150 mm 90° vertical notch model using (i) 10 kHz and (j) 150 kHz excitations; or 15 mm 150° inclined notch model using (k) 10 kHz and (l) 150 kHz excitations; or 75 mm inclined 150° inclined notch model using (m) 10 kHz and (n) 150 kHz excitations

### *5.2 Correlations*

The concrete notch depth and degree of inclination were divided by the major wavelength in order to offer a dimensionless relationship and provided a more general form that potentially suit any scale [16, 23, 24, 39-43]. The wavelength can be calculated using the common relation between velocity, wavelength, and dominant frequency. The dominant frequency, $f_D$ for each excitation frequency was computed based on the power spectrum density magnitude plot acquired from the FFT. Table 3 lists the calculated R-waves velocities and these values were used to compute the ratio between notch depth and wavelength, $d/\lambda$ as well as degree of inclination and wavelength, $\theta/\lambda$ for each excitation frequency.

**Table 3.** Velocity of R-waves generated by different excitation frequencies.

| Frequency of wave $f$, (kHz) | R-wave velocity (Steel reinforced concrete model)(m/s) |
|---|---|
| 10 | 2281.3 |
| 20 | 2361.2 |
| 30 | 2370.1 |
| 40 | 2375.7 |
| 50 | 2378.2 |
| 60 | 2381.3 |
| 80 | 2383.7 |
| 100 | 2390.0 |
| 150 | 2392.6 |

The power and logarithmic regressions derived from the plot of R-wave WT and phase velocity indices with respect to the ratio between notch depth and wavelength, $d/\lambda$ show good correlations, as presented in Figures 8 and 9. It is also found that both the WT and phase velocity indices decreased as the $d/\lambda$ increased with a slightly lower correlation compared to WT index. Taking WT analysis results of 10 kHz excitation as examples (concrete model with vertical 90° surface notch), the change of *WT* index with regards to $d/\lambda$ was noticeable, which changes from 0.54 to 0.016 as $d/\lambda$ increases from 0.13 to 0.67.

However, for *d/λ* values of greater than 1, the *WT* index change eventually reaches a plateau. From the analyses, it is revealed that higher excitation frequencies result in higher value of velocity or phase velocity. Similar findings were reported in previous studies, pointing that although higher frequency waves suffer from stronger attenuation than the lower frequency ones, their propagation velocity is faster in inhomogeneous media like concrete [44, 45]. When the excitation frequency is 10 kHz, 150 mm notch length seems to give the largest drop in R-wave velocity index, which was up to 21.3 %, 14.1 %, 18.4 %, 18.6 % and 15.2 % as compared to the one from sound concrete model for cases with vertical (90°) and inclined notches cases (30°, 60°, 120° and 150°), respectively. On the contraly, the smallest decrease of velocity index which is caused by the notch length of 30 mm, have marked a maximum of 8.4 %, 4.3 %, 6.1 %, 5.0 % and 6.4 % dropped for the same cases as mentioned before. It is noteworthy that the velocity index decreases with the increase in notch depth, justifying the fact that the waves have to take longer time or longer path way to reach the other side of notch for deeper notches.

The WT and phase velocity indices vs. *θ/λ* data are given in Figures 10 and 11. The WT and phase velocity indices exhibit power and logarithmic regressions, respectively, with respect to the ratio between notch angle and wavelength, with moderate correlation coefficients. It is obvious that for higher frequency, the WT index becomes lower due to the higher tendency of high frequency components to lose energy through adsorption, scattering and distortion by the notch. Similar findings have been reported previously [18], in which the penetration depth of R-wave is believed to be equivalent to the excitation wavelength. It is assumed that the wave is propagating in a straightforward path below the notch when the wavelength is greater than the notch depth. On the other hand, the other mode of propagation which involves reflection and scattering has occurred when the R-waves wavelength is smaller than the notch depth.

The WT index seems to lose their sensitivity against deeper notch depths. There are few reasons for this behavior. Amongst, the penetration depth of R-wave which is considered as equal to one wavelength. According to Aggelis and Shiotani [18], the amplitude of R-wave at the depth of one wavelength is around 6 % of the surface amplitude for ideal non-attenuative material with mechanical properties similar to concrete. However, the attenuation of concrete certainly has an effect in decreasing the penetration depth, something that is not fully accounted for in the numerical simulation of this study. Besides, the energy of the wave is not proportional to the amplitude but to the square of the amplitude. This implies that the majority of R-wave energy propagates in shallower zone. Hence, despite the fact that the wavelength can be larger than the notch, still the energy passing below the notch is insignificant and therefore, the waveform readings for the larger notches do not show much discrepancy [19].

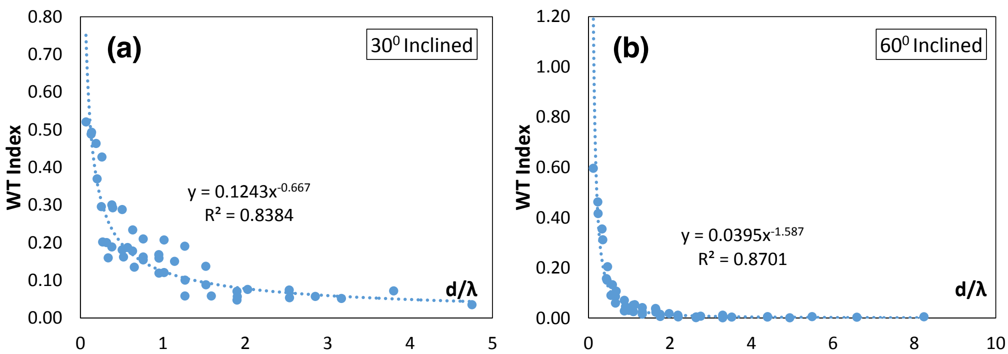

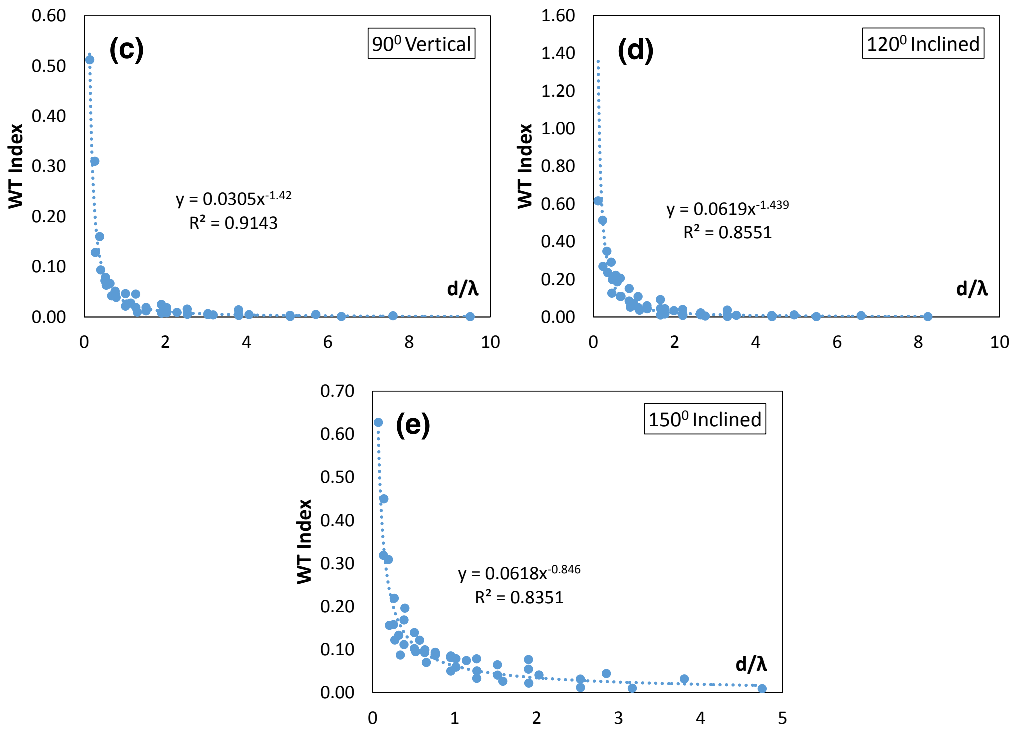


**Figure 8.** WT index versus *d/λ* for steel reinforced concrete model with (a) 30° inclined notch cases, (b) 60° inclined notch cases, (c) vertical notch (90° ) cases, (d) 120° inclined notch cases and (e) 150° inclined notch cases

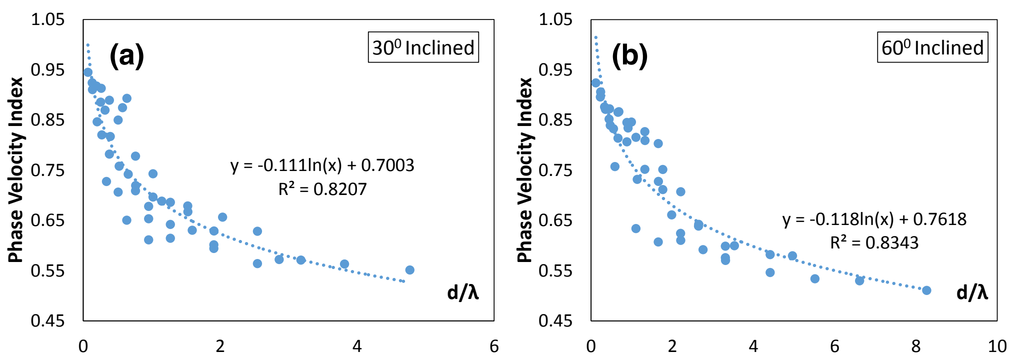

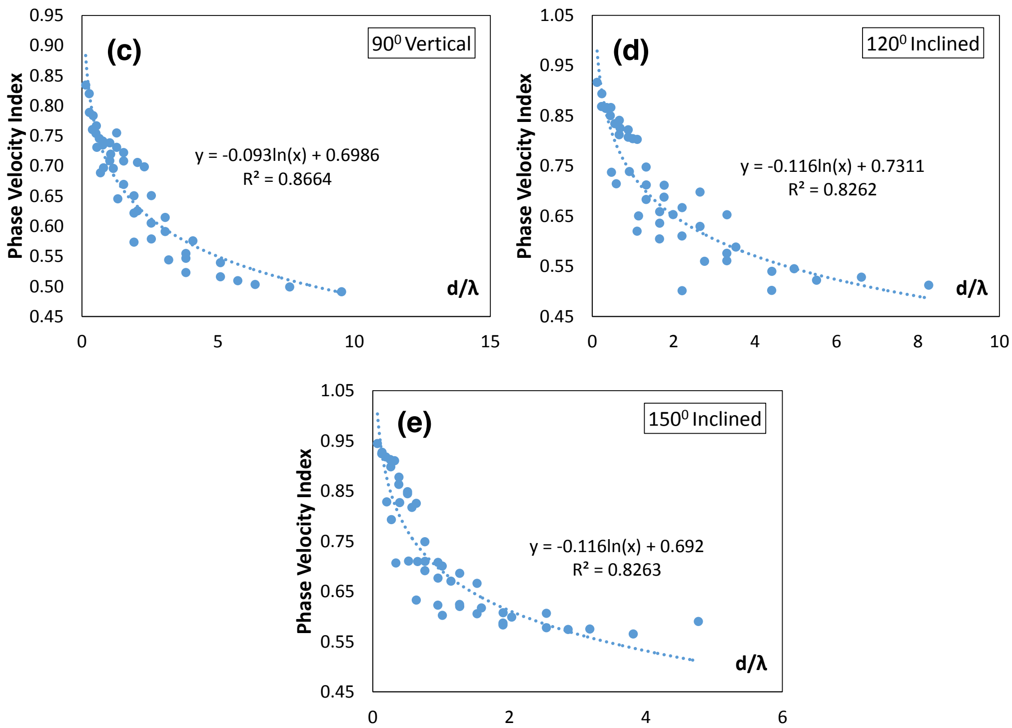


**Figure 9.** Phase velocity index versus *d/λ* for steel reinforced concrete model with (a) 30° inclined notch cases, (b) 60° inclined notch cases, (c) vertical (90°) cases, (d) 120° inclined notch cases and (e) 150° inclined notch cases

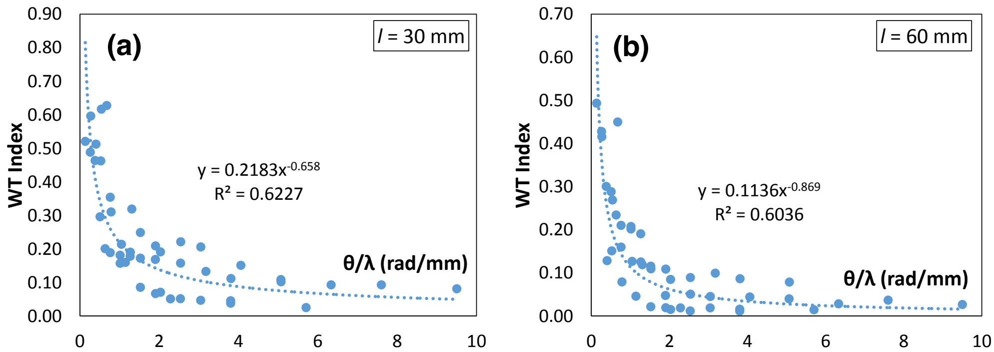

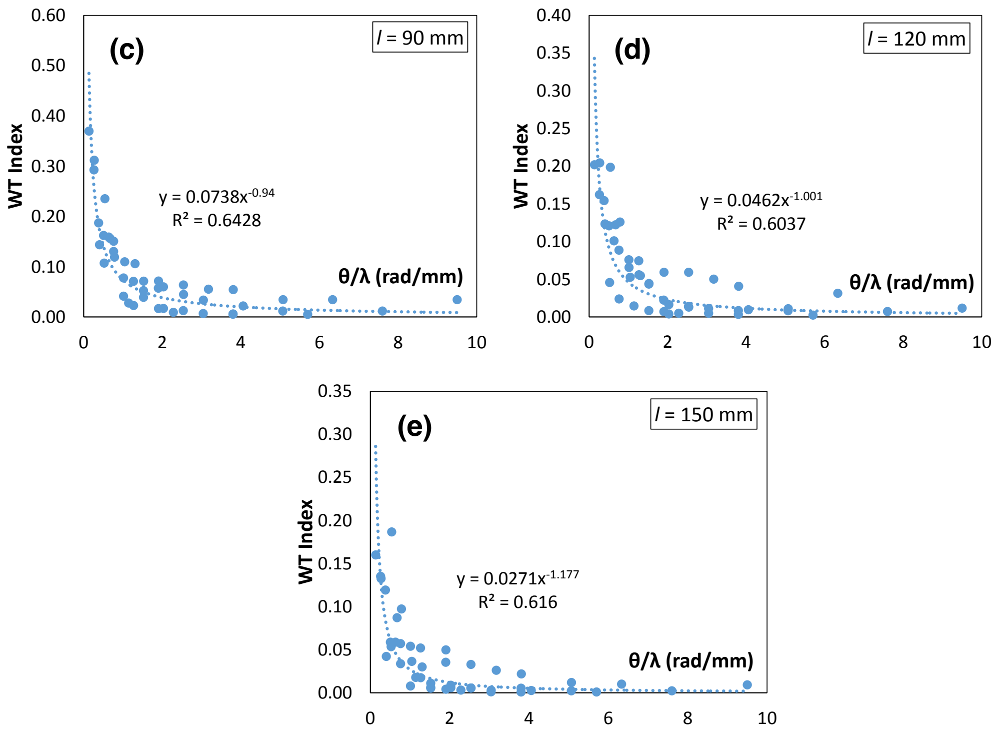


**Figure 10.** WT index versus $\theta/\lambda$ for steel reinforced concrete model with (a) 30 mm notch length cases, (b) 60 mm notch length cases, (c) 90 mm notch length cases, (d) 120 mm notch length cases and (e) 150 mm notch length cases

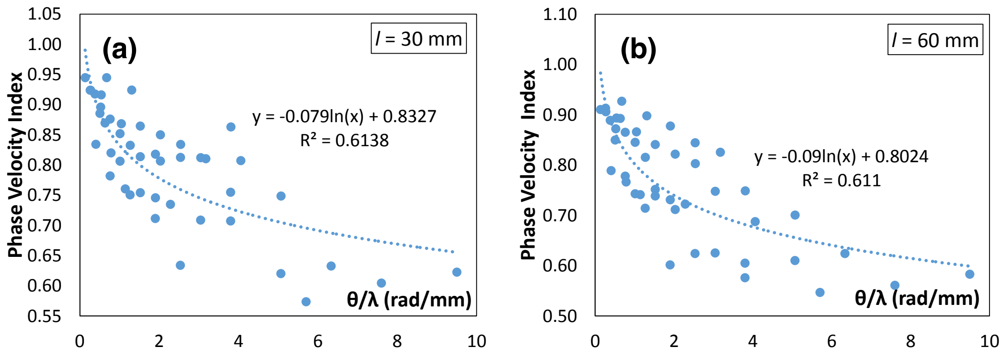


(a) (b)

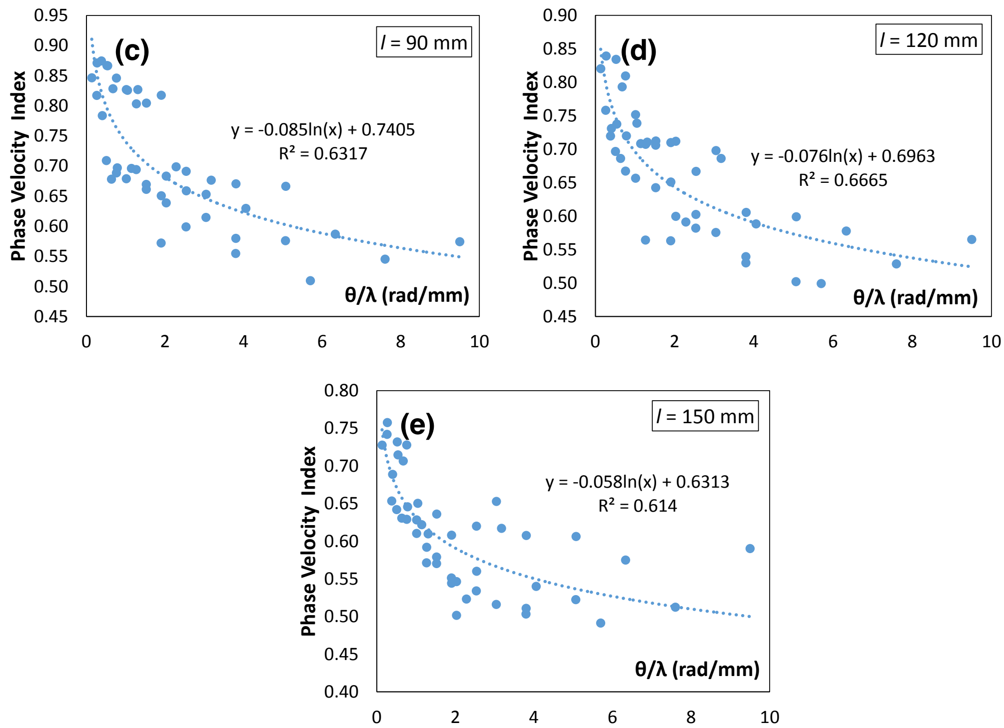


**Figure 11.** Phase velocity index versus *θ/λ* for steel reinforced concrete model with (a) 30 mm notch length cases, (b) 60 mm notch length cases, (c) 90 mm notch length cases, (d) 120 mm notch length cases and (e) 150 mm notch length cases

### *5.3 Experimental Results*

Five different diameters of steel balls (19 mm, 14 mm, 12 mm, 10 mm and 9 mm) were employed as impact sources in the experimental measurements, which exhibit consistent and broad spectral content of forcing function with dominant frequencies of 11.5 kHz, 13.1 kHz, 14.6 kHz, 18.2 kHz and 19.5 kHz, respectively. Examples of waveforms in steel reinforced concrete specimens obtained from tapping a 19 mm steel ball (dominant frequency of 11.7 kHz) against the face of concrete are depicted in Figure 12. Plotting the arrival time of R-wave obtained from each sensor with respect to distance, as seen in Figure 12, yields the propagation velocity which is the slope of the line. The arrival of R-waves arrival time is comparable to the one obtained from simulation. In addition, time domain traces measured at the same array arrangement for the specimen with inclined 30° (notch depth of 15 mm and 75 mm), and on vertical notch 90° (notch depth of 30 mm and 150 mm) as well as on inclined 150° (notch depth of 15 mm and 75 mm) depicted in Figures 13 (a) to (f) as well. Further, the processed experimental waveforms by MFCE for the same cases are showed as in Figure 14. As can be seen from the figure, the delay of Rayleigh peaks between S3 and S4 becomes longer when the depth of surface notch is increased. In addition, major reduction of amplitude is observable when compared the amplitude recorded from sensors after the notch to those recorded from sensors before the notch. The propagation of elastic wave may not be 'straight and direct' underneath the notch along the measurement array but it might traveled in other shorter paths in concrete medium and been diffracted by the notch tip.

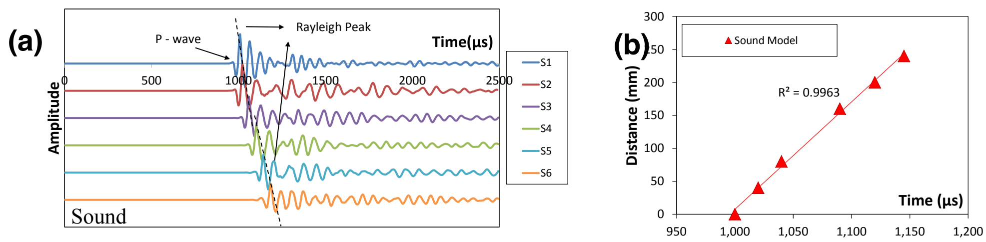


**Figure 12.** Experimental waveforms collected for (a) sound concrete specimen and (b) their corresponding R-waves propagation distance against arrival time. Excitations were done by 19 mm steel ball impact.

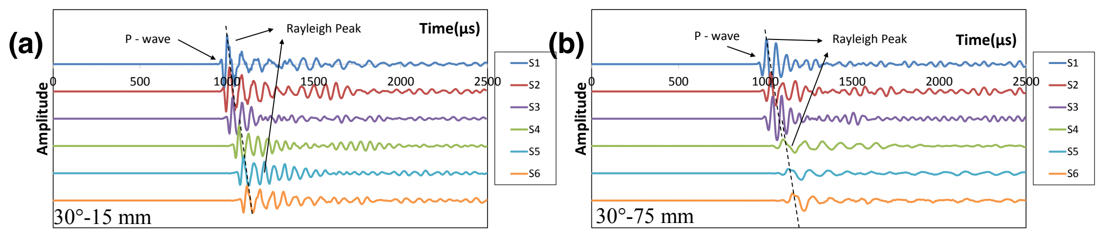

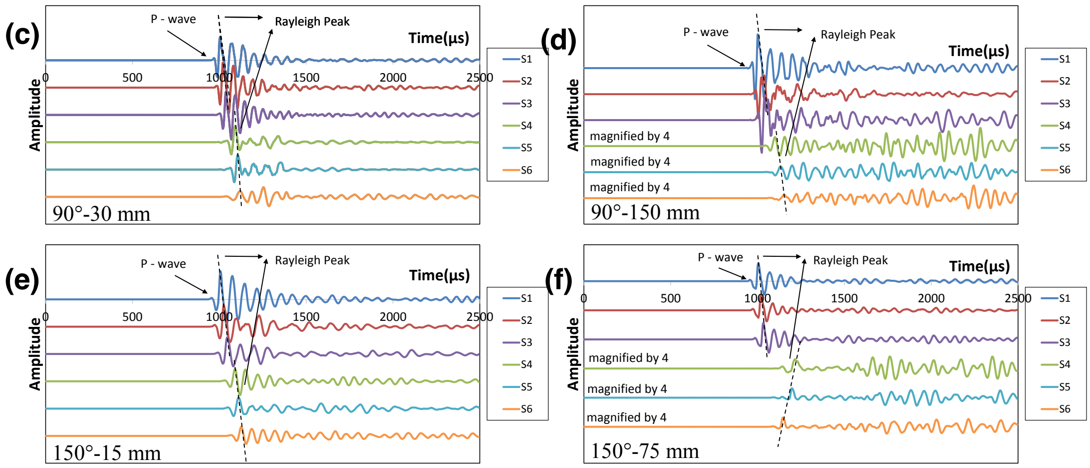


**Figure 13.** Experimental waveforms collected for (a) 15 mm 30° inclined notch, (b) 75 mm 30° inclined notch, (c) 30 mm 90° vertical notch, (d) 150 mm 90° vertical notch, (e) 15 mm 150° inclined notch and (f) 75 mm 150° inclined notch. Excitations were done by 19 mm steel ball impact.

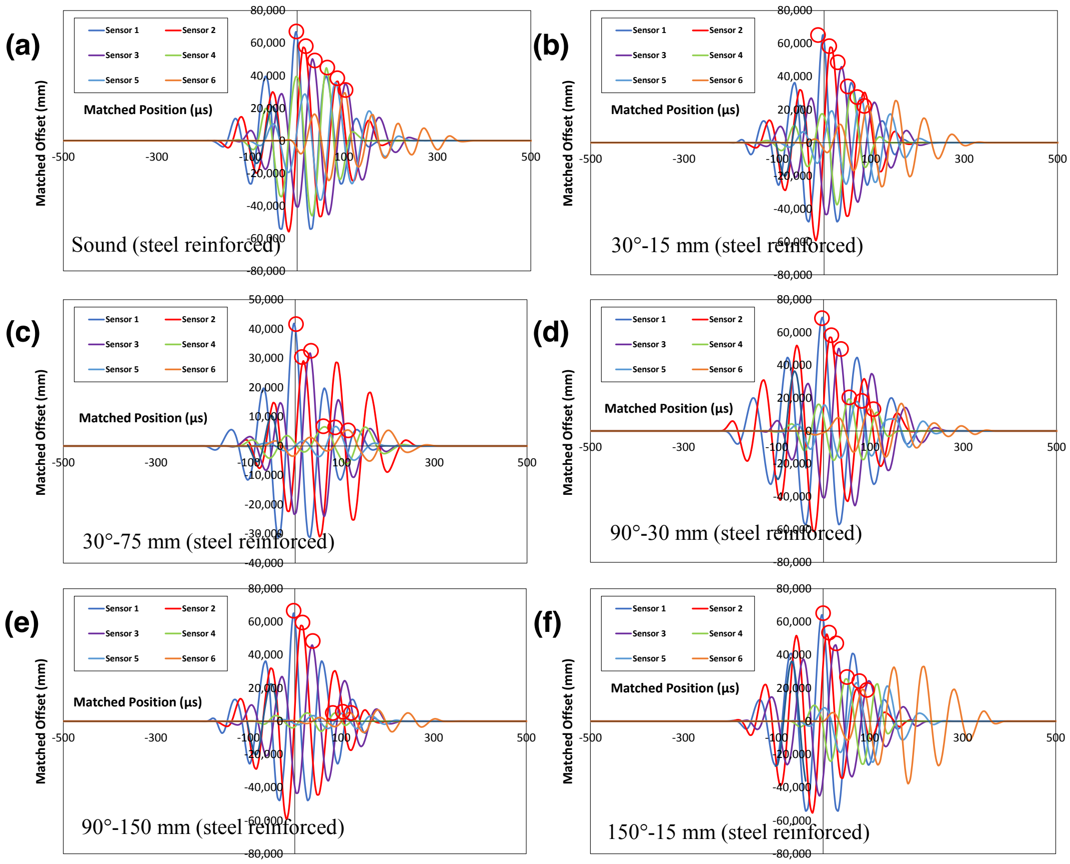

(g)

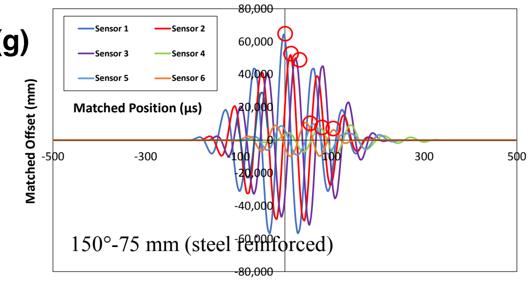


**Figure 14.** Processed experimental waveforms and the respective final R-wave peak matched positions based on MFCE method for (a) sound, (b) 15 mm 30° inclined notch, (c) 75 mm 30° inclined notch, (d) 30 mm 90° vertical notch, (e) 150 mm 90° vertical notch, (f) 15 mm 150° inclined notch and (g) 75 mm 150° inclined notch. Excitations were done by 19 mm steel ball impact.

The estimation results (based on the correlations established earlier) from experiment measurements were plotted against the actual notch depths and degree of inclinations for comparison, as shown in Figure 15. The actual values are indicated as scatter lines without marker, while the estimation values are represented by scatter lines with marker. The maximum and minimum discrepancies between the actual and estimated values for WT and phase velocity indices were given in Table 4. The notch depth estimation is found to be more accurate than the degree of inclination estimation. Apart from that, the performance of WT index is also more satisfactory than the phase velocity index with lower discrepancies. This can be explained by their higher $R^2$ values in the correlations established between the indices with the ratio of notch depth-to wavelength as well as with the degree of inclination. From the numerical estimation results, fluctuations were noted especially for the cases of notch depths of 120 mm and 150 mm and degree of inclinations of 120° and 150°.

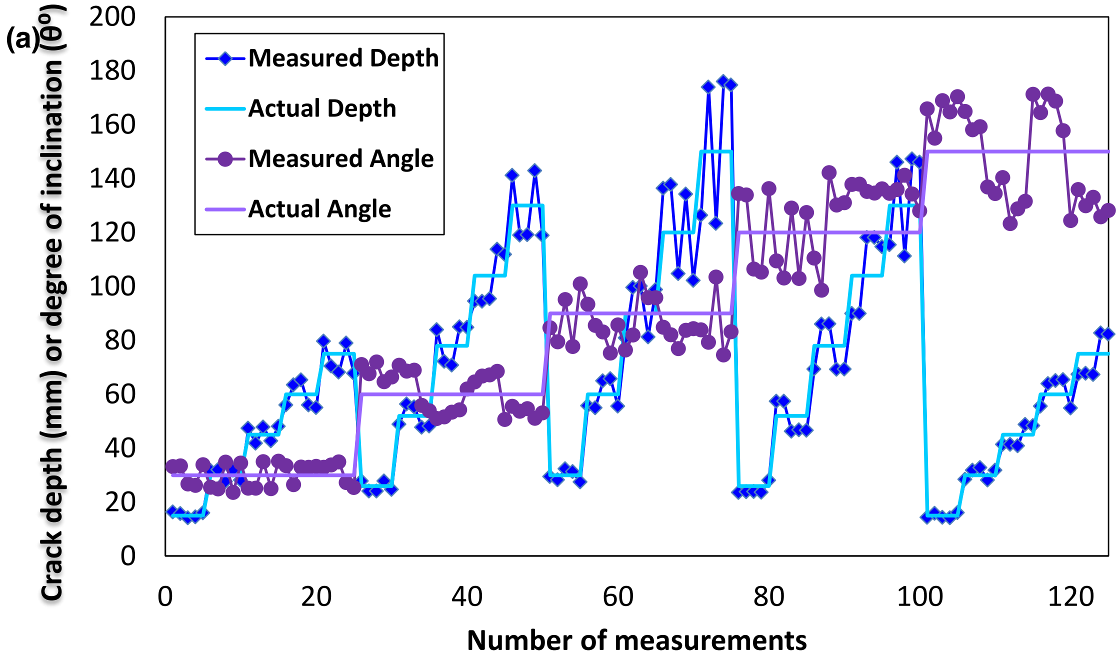


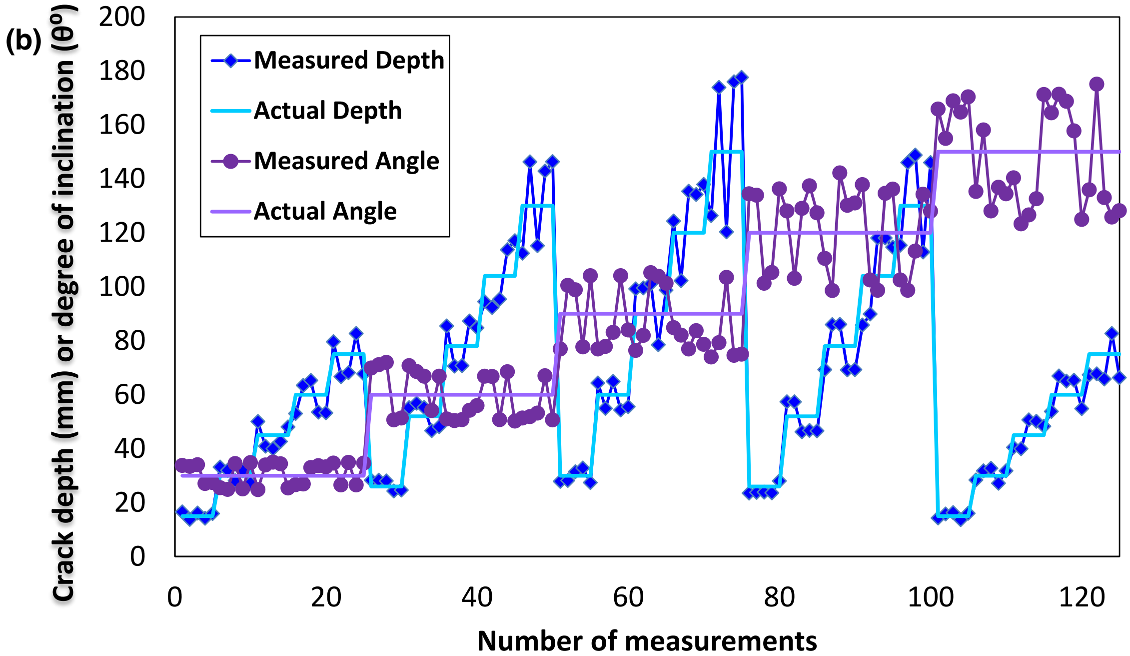


**Figure 15.** Surface notch depth and degree of inclination estimations based on (a) WT index (b) phase velocity index.

**Table 4.** Discrepancy between actual and estimation values for surface notch

| Index | Discrepancy between actual and estimated values (%) | | | |
|---|---|---|---|---|
| | Depth | | Angle | |
| | Max. | Min. | Max. | Min. |
| WT | 17.8 | 2.1 | 21.4 | -3.2 |
| Average | 8.8 | | 11.7 | |
| Phase velocity | 19.8 | -3.6 | -19.9 | -3.3 |
| Average | 9.8 | | 12.8 | |

*a negative value indicates over-estimation and vice versa

## 6. Conclusions

In the present work, the behavior of R-waves propagating reinforced concrete with a surface notch is investigated both numerically and experimentally in a more systematic manner. The study is focused on the WT coefficient and phase velocity changes of the R-waves and their dependence on depth and inclination. Multichannel acquisition procedure was developed in the study to record the propagating elastic waves, extract and analyze for the R-wave components. Correlations between the specific R-wave parameters with the ratios of notch depth, degree of inclination and wavelength were established. The accuracy of the correlations was verified through experimental measurements on concrete specimens induced with surface notch. In general measurement results gave satisfactory agreement between the proposed WT and phase velocity indices and notch depth as well as its degree of inclination, making them reliable parameters for quantifying and characterizing concrete surface notch, particularly when the wavelength is greater than the notch depth. The proposed R-wave measurement and assessment methodology can possibly be refined for enhanced reliability and practicality. Its feasibility for in-situ applications could be justified through methods such as coring. Future work will be focused on confirming the addition effect by a real crack as compared to a notch. Additional parameter or factor may be proposed to the correlations to cater for this effect. In addition, a more steady study should also be conducted on developing classification method to characterize surface notch depth and orientation simultaneously, such as the artificial neural network.

**Acknowledgments**

This work was supported under the Ministry of Education Malaysia-High Impact Research (MOHE-HIR) UM.C/625/1/HIR/MOHE/ENG/54, University of Malaya Research Grant Scheme RP004B-13AET and partially supported by PRGS (PR001-2015A). Special appreciation is expressed to MDC Precast Industries Sdn Bhd (501872-A) for the experimental supports.

**References**

1. Chai, H. K., Momoki, S., Kobayashi, Y., Aggelis, D. G., & Shiotani, T. (2011). Tomographic reconstruction for concrete using attenuation of ultrasound. *NDT & E International*, *44*(2), 206-215.
2. Zhu, J. (2008). *Non-contact NDT of concrete structures using air coupled sensors*. Newmark Structural Engineering Laboratory. University of Illinois at Urbana-Champaign.
3. Shin, S.W (2008). *Elastic Rayleigh Wave for Nondestructive Health Monitoring of Concrete Structure*. VDM Verlag Dr. Muller: Germany.
4. Goueygou, M., Lafhaj, Z., & Soltani, F. (2009). Assessment of porosity of mortar using ultrasonic Rayleigh waves. *NdT & E International*, *42*(5), 353-360.
5. In, C. W., Kim, J. Y., Kurtis, K. E., & Jacobs, L. J. (2009). Characterization of ultrasonic Rayleigh surface waves in asphaltic concrete. *NDT & E International*, *42*(7), 610-617.

6. Alver, N., & Ohtsu, M. (2013). Nondestructive Evaluation of Surface Crack Depth in Concrete. In *Topics in Dynamics of Civil Structures, Volume 4* (pp. 269-275). Springer New York.
7. Lai, W. L., Wang, Y. H., Kou, S. C., & Poon, C. S. (2013). Dispersion of ultrasonic guided surface wave by honeycomb in early-aged concrete. *NDT & E International*, *57*, 7-16.
8. Kim, G., In, C. W., Kim, J. Y., Kurtis, K. E., & Jacobs, L. J. (2014). Air-coupled detection of nonlinear Rayleigh surface waves in concrete—Application to microcracking detection. *NDT & E International*, *67*, 64-70.
9. Wang, C. Y., Liao, S. T., Tong, J. H., & Chiu, C. L. (2015). Numerical and experimental study on multi-directional SAFT to detect defects inside plain or reinforced concrete. *Construction and Building Materials*, *76*, 351-359.
10. Song, W. J., Popovics, J. S., Aldrin, J. C., & Shah, S. P. (2003). Measurement of surface wave transmission coefficient across surface-breaking cracks and notches in concrete. *The Journal of the Acoustical Society of America*, *113*(2), 717-725.
11. Kee, S. H., & Zhu, J. (2010). Using air-coupled sensors to determine the depth of a surface-breaking crack in concrete. *The Journal of the Acoustical Society of America*, *127*(3), 1279-1287.
12. Kee, S. H., & Zhu, J. (2011). Effects of sensor locations on air-coupled surface wave transmission measurements across a surface-breaking crack. IEEE transactions on ultrasonics, ferroelectrics, and frequency control, 58(2), 427-436.
13. Kee, S. H., & Zhu, J. (2014). Surface Wave Transmission across a Partially Closed Surface-Breaking Crack in Concrete. *ACI Materials Journal*, *111*(1).

14. In, C. W., Schempp, F., Kim, J. Y., & Jacobs, L. J. (2015). A Fully Non-contact, Air-Coupled Ultrasonic Measurement of Surface Breaking Cracks in Concrete. *Journal of Nondestructive Evaluation*, *34*(1), 1-7.
15. Chai, H. K., Momoki, S., Aggelis, D. G., & Shiotani, T. (2010). Characterization of Deep Surface-Opening Cracks in Concrete: Feasibility of Impact-Generated Rayleigh-Waves. *ACI Materials Journal*, *107*(3).
16. Zerwer, A., Polak, M. A., & Santamarina, J. C. (2005). Detection of surface breaking cracks in concrete members using Rayleigh waves. *Journal of Environmental & Engineering Geophysics*, *10*(3), 295-306.
17. Shiotani, T. (2006). Evaluation of repair effect for deteriorated concrete piers of intake dam using AE activity. In Advanced Materials Research (Vol. 13, pp. 175-180). Trans Tech Publications.
18. Aggelis, D. G., & Shiotani, T. (2007). Repair evaluation of concrete cracks using surface and through-transmission wave measurements. *Cement and Concrete Composites*, *29*(9), 700-711.
19. Aggelis, D. G., Shiotani, T., & Polyzos, D. (2009). Characterization of surface crack depth and repair evaluation using Rayleigh waves. Cement and Concrete Composites, 31(1), 77-83.
20. Shiotani, T., Momoki, S., Chai, H., & Aggelis, D. G. (2009). Elastic wave validation of large concrete structures repaired by means of cement grouting.*Construction and Building Materials*, *23*(7), 2647-2652.
21. Lee, F. W., Lim, K. S., & Chai, H. K. (2016). Determination and extraction of Rayleigh-waves for concrete cracks characterization based on matched filtering of center of energy. *Journal of Sound and Vibration*, *363*, 303-315.

22. Lee, F. W., Chai, H. K., & Lim, K. S. (2016). Assessment of Reinforced Concrete Surface Breaking Crack Using Rayleigh Wave Measurement. *Sensors*, *16*(3), 337.
23. Popovics, S. (2001). Analysis of the concrete strength versus ultrasonic pulse velocity relationship. *Materials Evaluation*, *59*(2), 123-130.
24. Shah, S. P., Popovics, J. S., Subramaniam, K. V., & Aldea, C. M. (2000). New directions in concrete health monitoring technology. *Journal of engineering mechanics*, *126*(7), 754-760.
25. Wave2000, Cyber-Logic, Inc., New York, http://www.cyberlogic.org.
26. Kaufman, J. J., Luo, G., & Siffert, R. S. (2008). Ultrasound simulation in bone. *ieee transactions on ultrasonics, ferroelectrics, and frequency control*,*55*(6), 1205-1218.
27. Aggelis, D. G., Tsimpris, N., Chai, H. K., Shiotani, T., & Kobayashi, Y. (2011). Numerical simulation of elastic waves for visualization of defects.*Construction and Building Materials*, *25*(4), 1503-1512.
28. Chai, H. K., Momoki, S., Aggelis, D. G., Kobayashi, Y., & Shiotani, T. (2010). Recent development in tomography techniques for non-destructive evaluation of concrete. In *Proceedings of the Second Asia-Pacific Young Researchers and Graduates Symposium (YRGS 2010)* (pp. 10-18).
29. Sachse, W., & Pao, Y. H. (1978). On the determination of phase and group velocities of dispersive waves in solids. *Journal of Applied Physics*, *49*(8), 4320-4327.
30. Kishimoto, K., Inoue, H., Hamada, M., & Shibuya, T. (1995). Time frequency analysis of dispersive waves by means of wavelet transform. *Journal of Applied Mechanics*, *62*(4), 841-846.
31. Kim, Y. Y., & Kim, E. H. (2001). Effectiveness of the continuous wavelet transform in the analysis of some dispersive elastic waves. *The Journal of the Acoustical Society of America*, *110*(1), 86-94.

32. Quek, S. T., Wang, Q., Zhang, L., & Ong, K. H. (2001). Practical issues in the detection of damage in beams using wavelets. *Smart Materials and Structures*, *10*(5), 1009.
33. Wang, L., & Yuan, F. G. (2007). Group velocity and characteristic wave curves of Lamb waves in composites: Modeling and experiments. *Composites science and technology*, *67*(7), 1370-1384.
34. Song, F., Huang, G. L., Kim, J. H., & Haran, S. (2008). On the study of surface wave propagation in concrete structures using a piezoelectric actuator/sensor system. *Smart materials and Structures*, *17*(5), 055024.
35. Gaul, L., & Hurlebaus, S. (1998). Identification of the impact location on a plate using wavelets. *Mechanical Systems and Signal Processing*, *12*(6), 783-795.
36. Suzuki, H., Kinjo, T., Hayashi, Y., Takemoto, M., Ono, K., & Hayashi, Y. (1996). Wavelet transform of acoustic emission signals. *Journal of Acoustic Emission*, *14*, 69-84.
37. Sansalone, M. J., & Streett, W. B. (1997). Impact-echo. Nondestructive evaluation of concrete and masonry.
38. Yew, C. H., Chen, K. G., & Wang, D. L. (1984). An experimental study of interaction between surface waves and a surface breaking crack. *The Journal of the Acoustical Society of America*, *75*(1), 189-196.
39. Doyle, P. A., & Scala, C. M. (1978). Crack depth measurement by ultrasonics: a review. *Ultrasonics*, *16*(4), 164-170.
40. Hevin, G., Abraham, O., Pedersen, H. A., & Campillo, M. (1998). Characterization of surface cracks with Rayleigh waves: a numerical model.*NDT & E International*, *31*(4), 289-297.

41. Pecorari, C. (1998). Rayleigh wave dispersion due to a distribution of semi-elliptical surface-breaking cracks, *The Journal of the Acoustical Society of America*, Vol. 103, No. 3, pp. 1383-1387.

42. Pecorari, C. (2001). Scattering of a Rayleigh wave by a surface-breaking crack with faces in partial contact, *Wave Motion*, Vol. 33, No. 3, pp. 259-270.

43. Tsutsumi, T., Wu, J., Wu, J., Huang, X., & Wu, Z. (2005). Introduction to a new surface-wave based NDT method for crack detection and its application in large dam monitoring, *Proceedings of international symposium on dam safety and detection of hidden troubles of dams and dikes*, Xian, China, pp. 1-3.

44. Philippidis, T. P., & Aggelis, D. G. (2005). Experimental study of wave dispersion and attenuation in concrete. Ultrasonics, 43(7), 584-595.

45. Chaix, J. F., Garnier, V., & Corneloup, G. (2006). Ultrasonic wave propagation in heterogeneous solid media: Theoretical analysis and experimental validation. Ultrasonics, 44(2), 200-210.

Figure
Click here to download Figure: Figure 1.docx

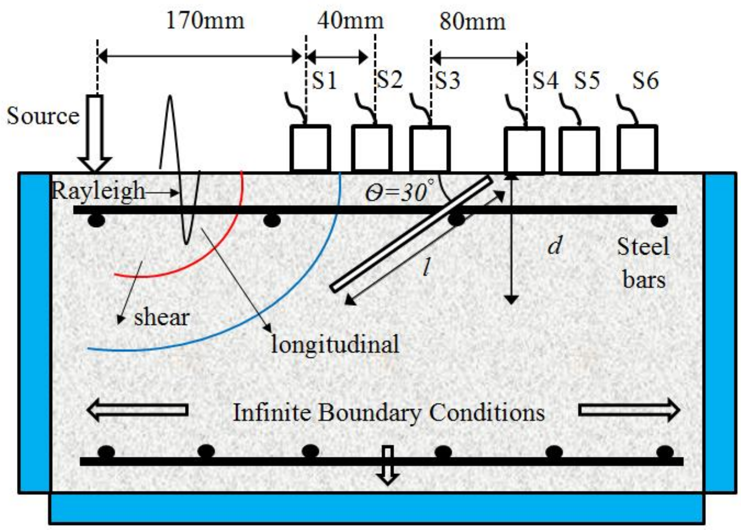


**Figure 1.** Wave motion simulation model.

Figure
Click here to download Figure: Figure 2.docx

**Figure 2.** Photograph of accelerometer sensors arranged on the upper side of concrete specimen.

**Figure**

**Click here to download Figure: Figure 3.docx**

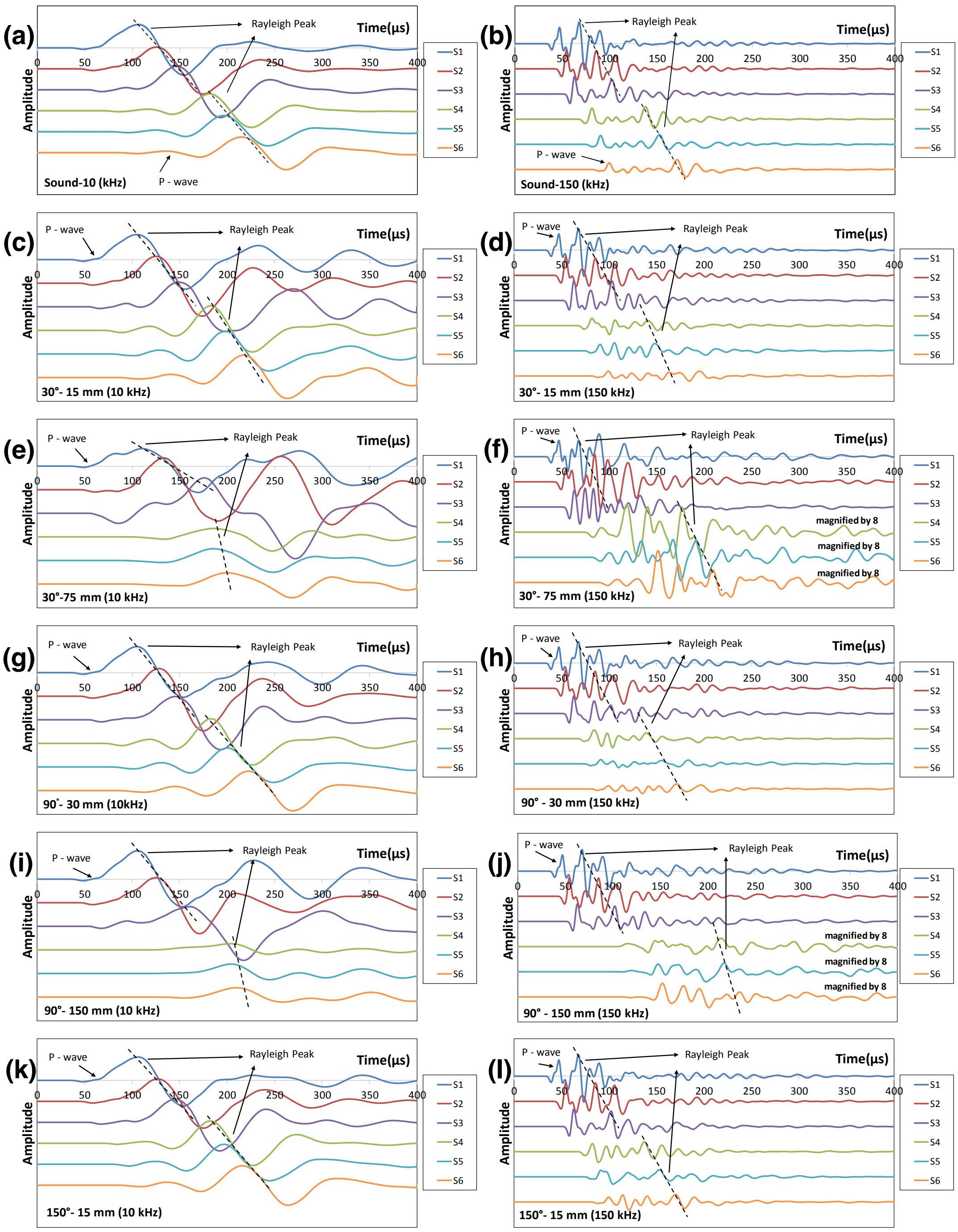

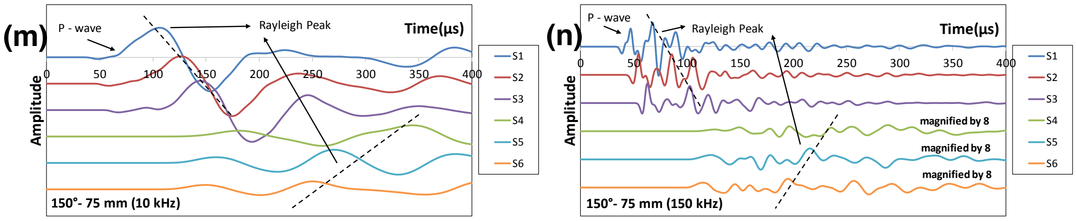


**Figure 3.** Simulated waveforms collected from steel reinforced concrete model for sound concrete mode using (a) 10 kHz and (b) 150 kHz excitations; 15 mm 30° inclined notch using (c) 10 kHz and (d) 150 kHz excitations; for 75 mm 30° inclined notch using (e) 10 kHz and (f) 150 kHz excitations; for 30 mm 90° vertical notch using (g) 10 kHz and (h) 150 kHz excitations; for 150 mm 90° vertical notch using (i) 10 kHz and (j) 150 kHz excitations; for 15 mm 150° inclined notch using (k) 10 kHz and (l) 150 kHz excitations; for 75 mm 150° inclined notch using (m) 10 kHz and (n) 150 kHz excitations

**Figure**
Click here to download Figure: Figure 4.docx

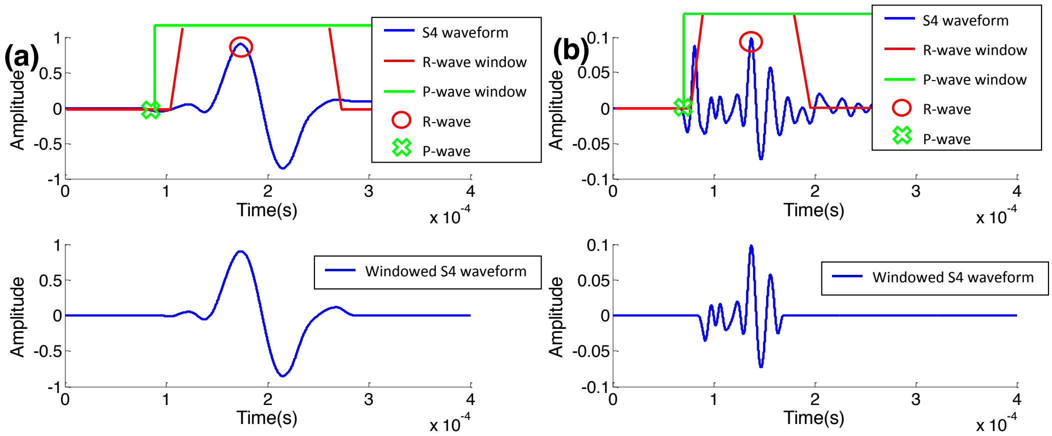


**Figure 4.** Processing of waveforms using proposed matched filtering algorithm from sensor S4 for sound steel reinforced concrete model using (a) 10 kHz and (b) 150 kHz excitations

Figure

Click here to download Figure: Figure 5.docx

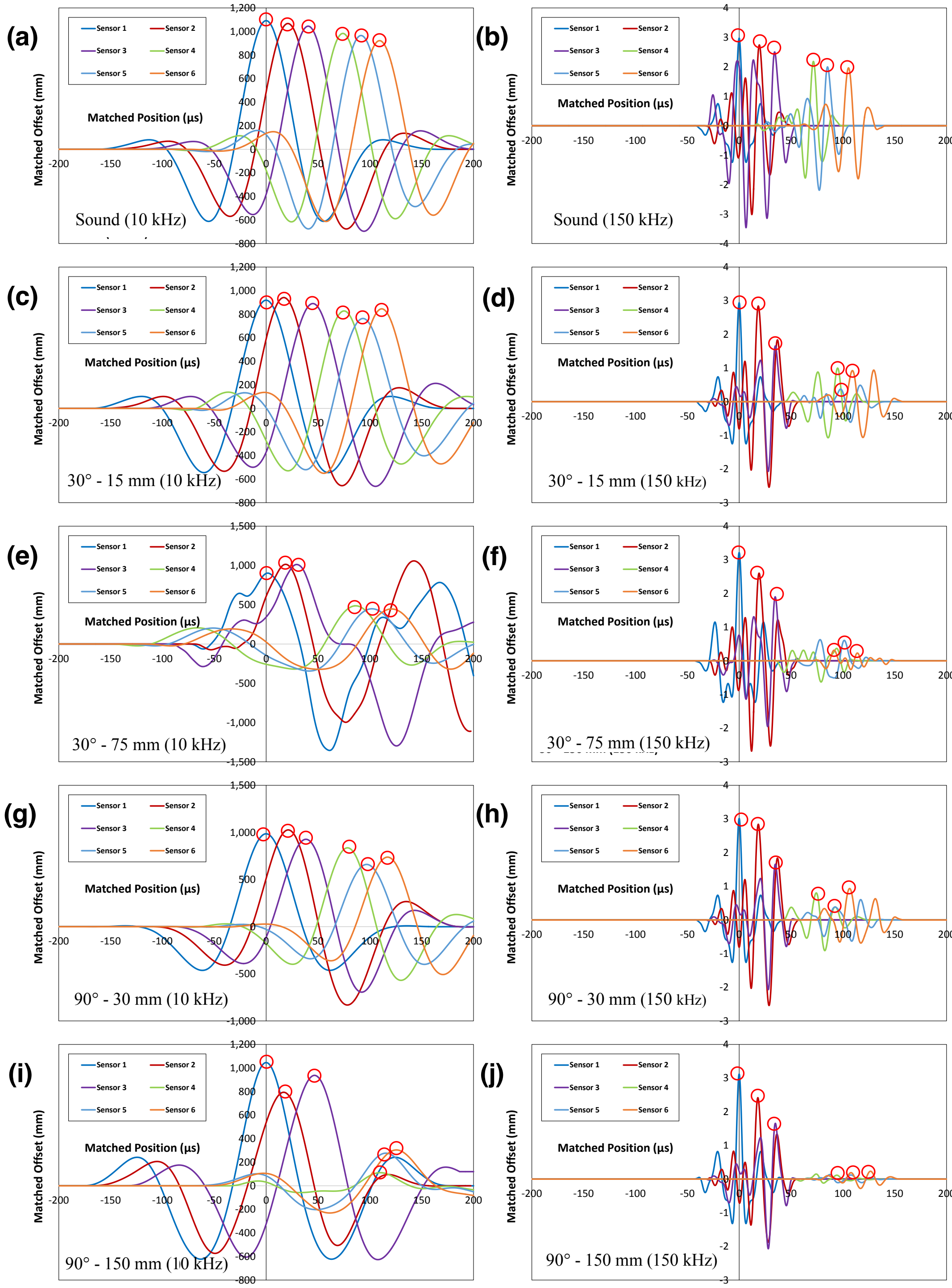

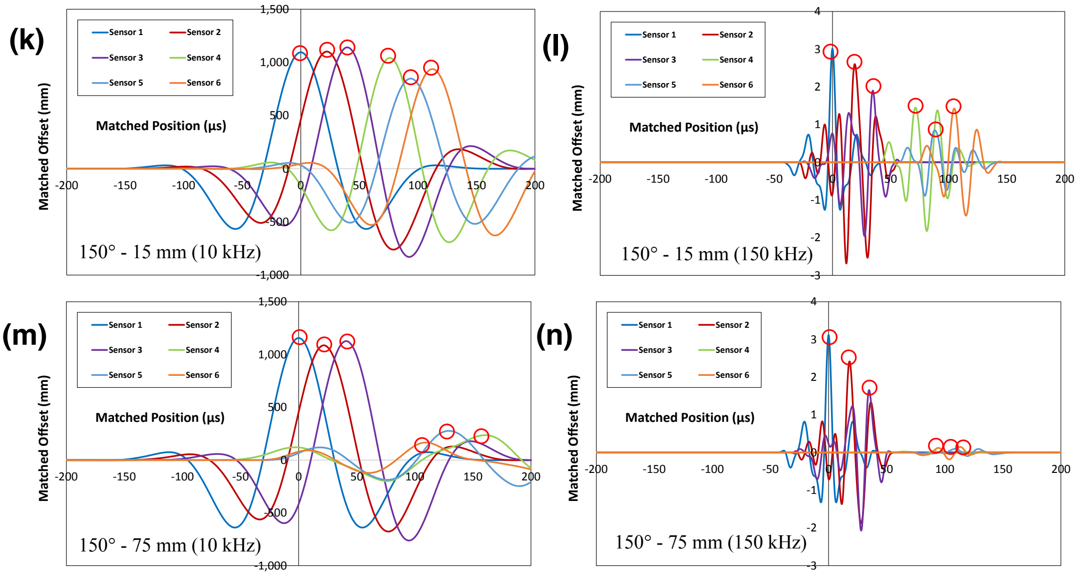


**Figure 5.** Processed waveforms and the respective final R-wave peak matched positions based on MFCE method for sound concrete model using (a) 10 kHz and (b) 150 kHz excitations; for 15 mm 30° inclined notch using (c) 10 kHz and (d) 150 kHz excitations; for 75 mm 30° inclined notch using (e) 10 kHz and (f) 150 kHz excitations; for 30 mm 90° vertical notch using (g) 10 kHz and (h) 150 kHz excitations; for 150 mm 90° vertical notch using (i) 10 kHz and (j) 150 kHz excitations; for 15 mm 150° inclined notch using (k) 10 kHz and (l) 150 kHz excitations; for 75 mm 150° inclined notch using (m) 10 kHz and (n) 150 kHz excitations

Figure
Click here to download Figure: Figure 6.docx

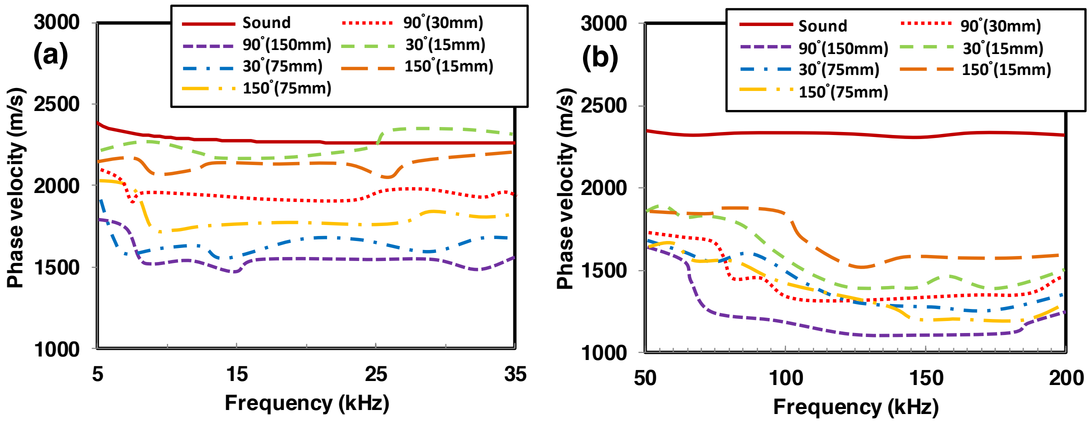


**Figure 6.** Dispersion curve computed for sound and various surface notched concrete models using (a) 10 kHz and (b) 150 kHz excitations

Figure

Click here to download Figure: Figure 7.docx

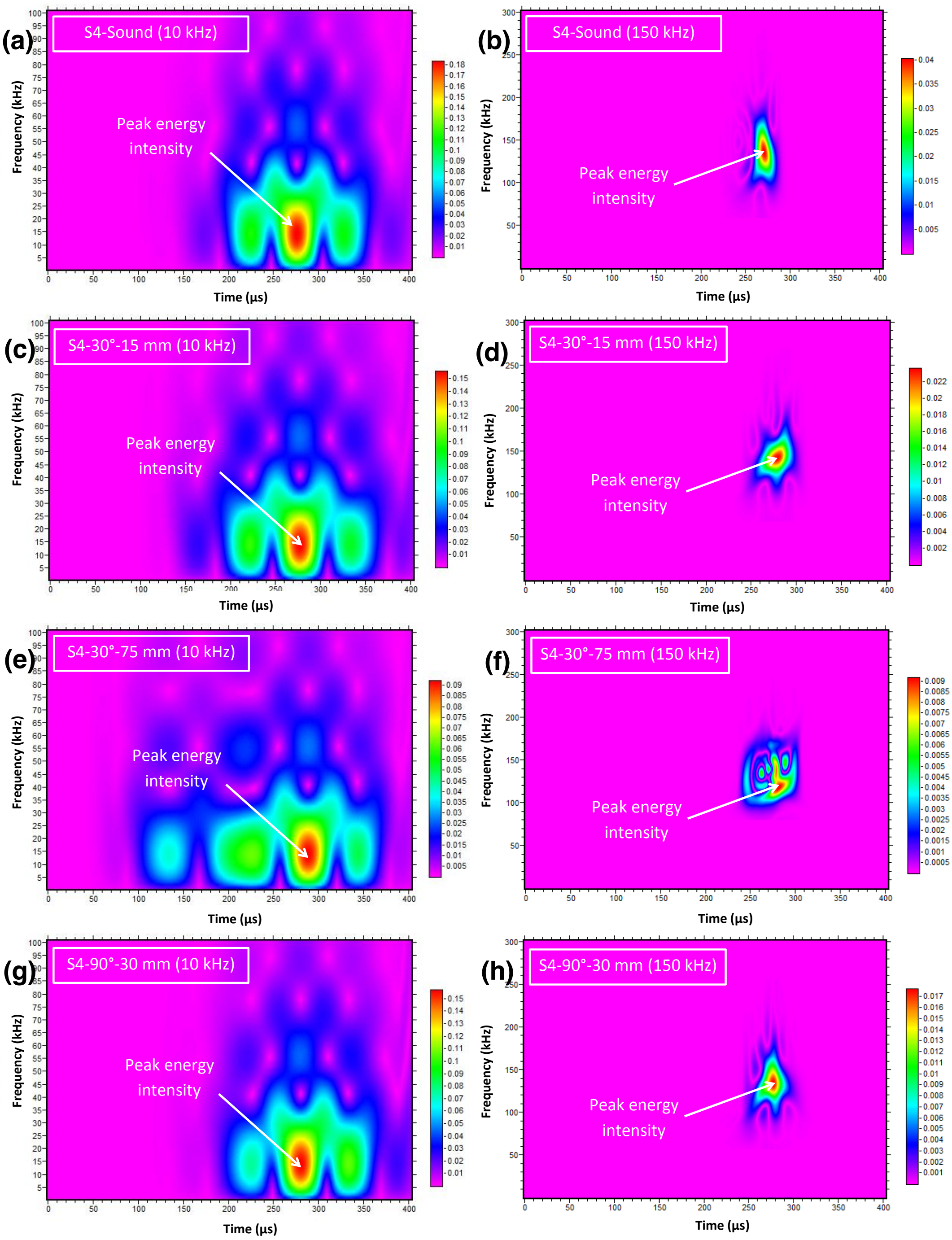

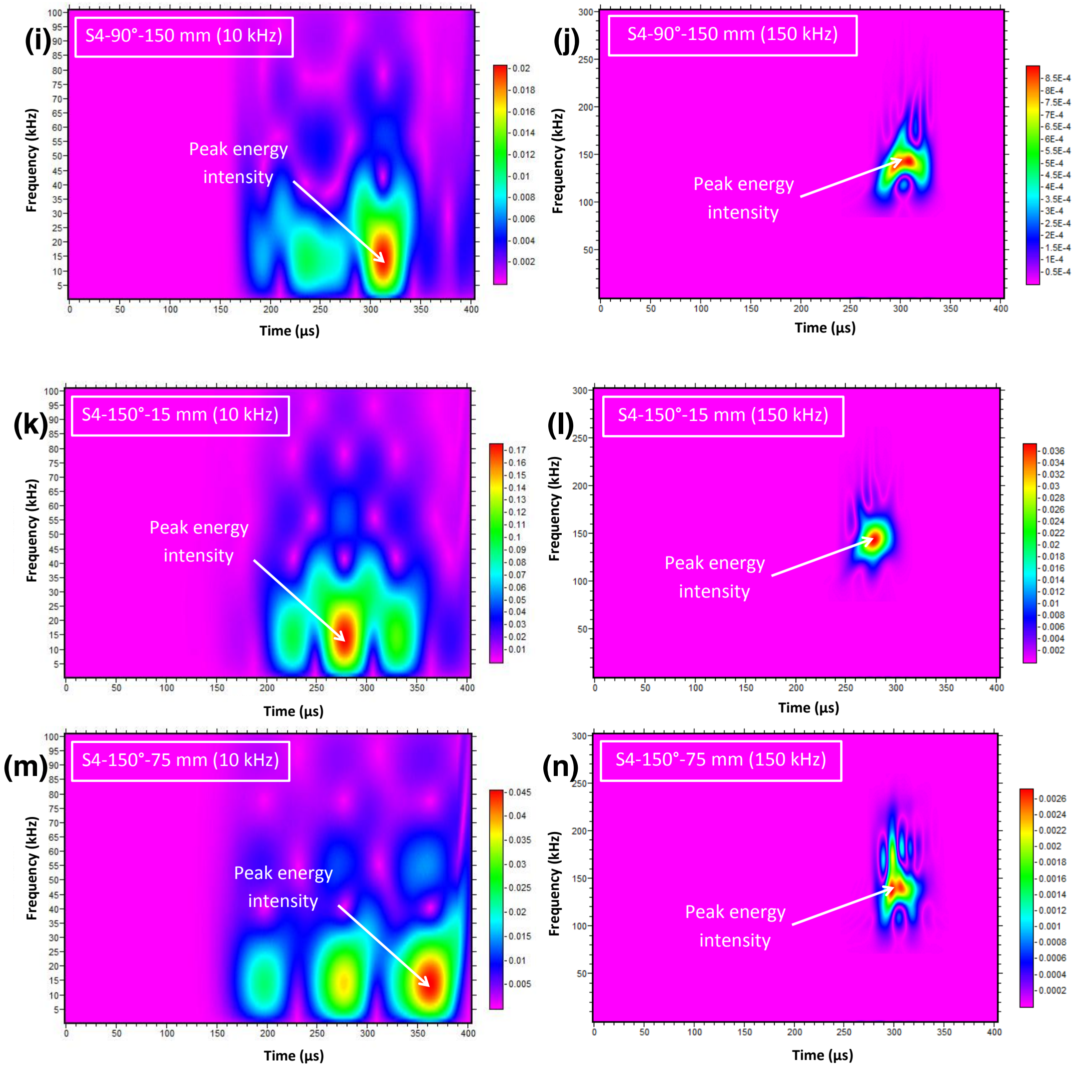


**Figure 7.** 2D wavelet transform contour diagram at the fourth sensors (S4) for steel reinforced concrete model using (a) 10 kHz and (b) 150 kHz; for 15 mm 30° inclined notch model using (c) 10 kHz and (d) 150 kHz excitations; for 75 mm 30° inclined notch model using (e) 10 kHz and (f) 150 kHz excitations; or 30 mm 90° vertical notch model using (g) 10 kHz and (h) 150 kHz excitations; for 150 mm 90° vertical notch model using (i) 10 kHz and (j) 150 kHz excitations; or 15 mm 150° inclined notch model using (k) 10 kHz and (l) 150 kHz excitations; or 75 mm inclined 150° inclined notch model using (m) 10 kHz and (n) 150 kHz excitations

**Figure**
**Click here to download Figure: Figure 8.docx**

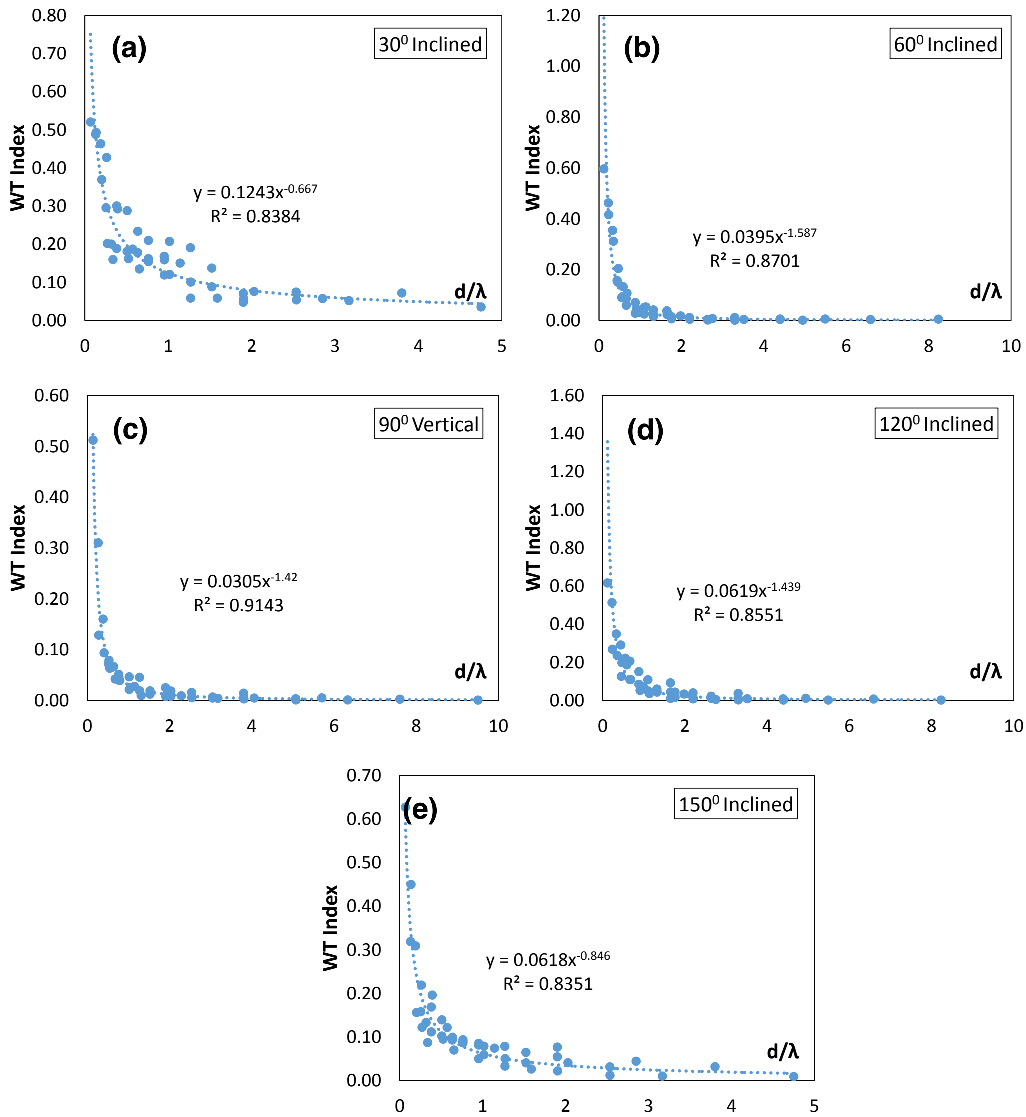


**Figure 8.** WT index versus *d/λ* for steel reinforced concrete model with (a) 30° inclined notch cases, (b) 60° inclined notch cases, (c) vertical notch (90° ) cases, (d) 120° inclined notch cases and (e) 150° inclined notch cases

**Figure**
**Click here to download Figure: Figure 9.docx**

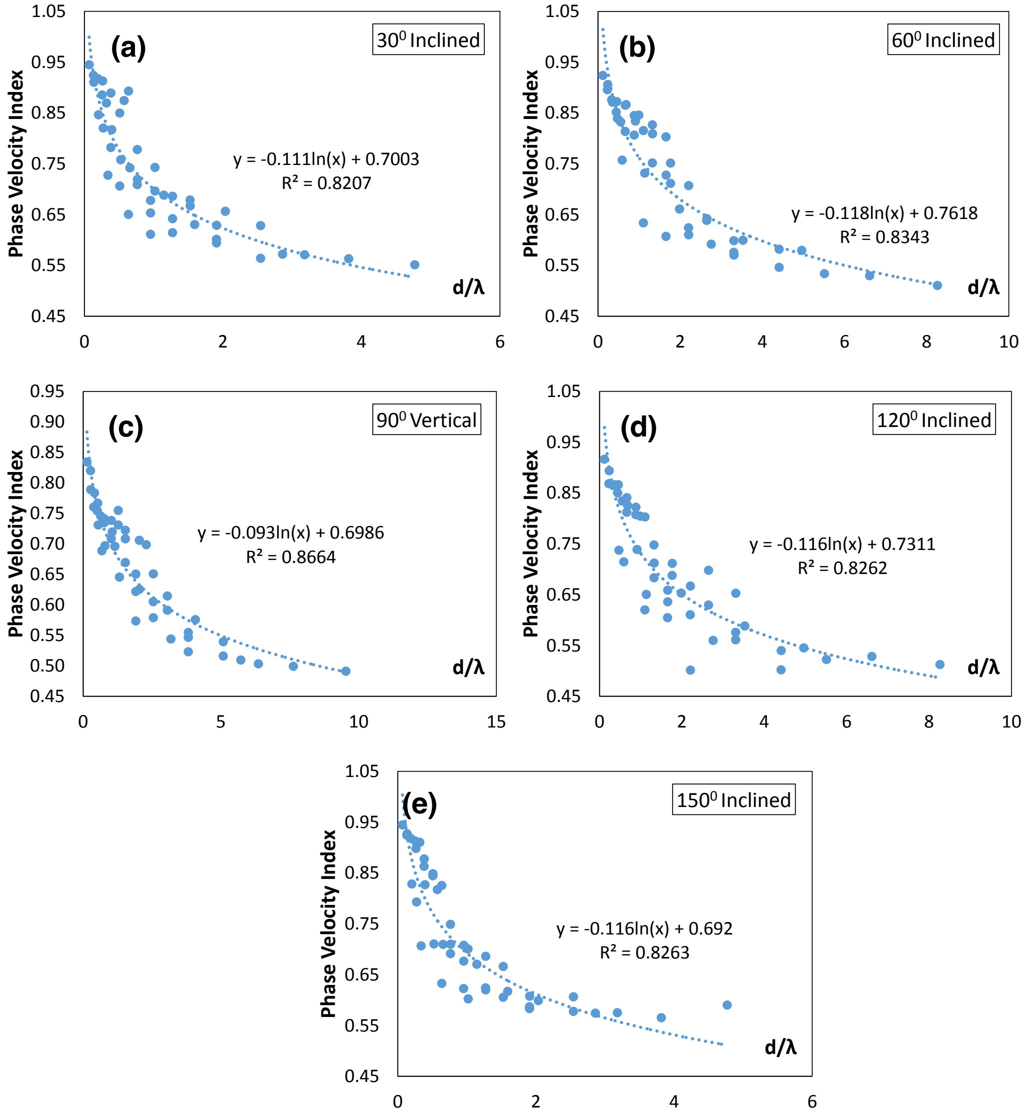


**Figure 9.** Phase velocity index versus *d/λ* for steel reinforced concrete model with (a) 30° inclined notch cases, (b) 60° inclined notch cases, (c) vertical (90°) cases, (d) 120° inclined notch cases and (e) 150° inclined notch cases

Figure

Click here to download Figure: Figure 10.docx

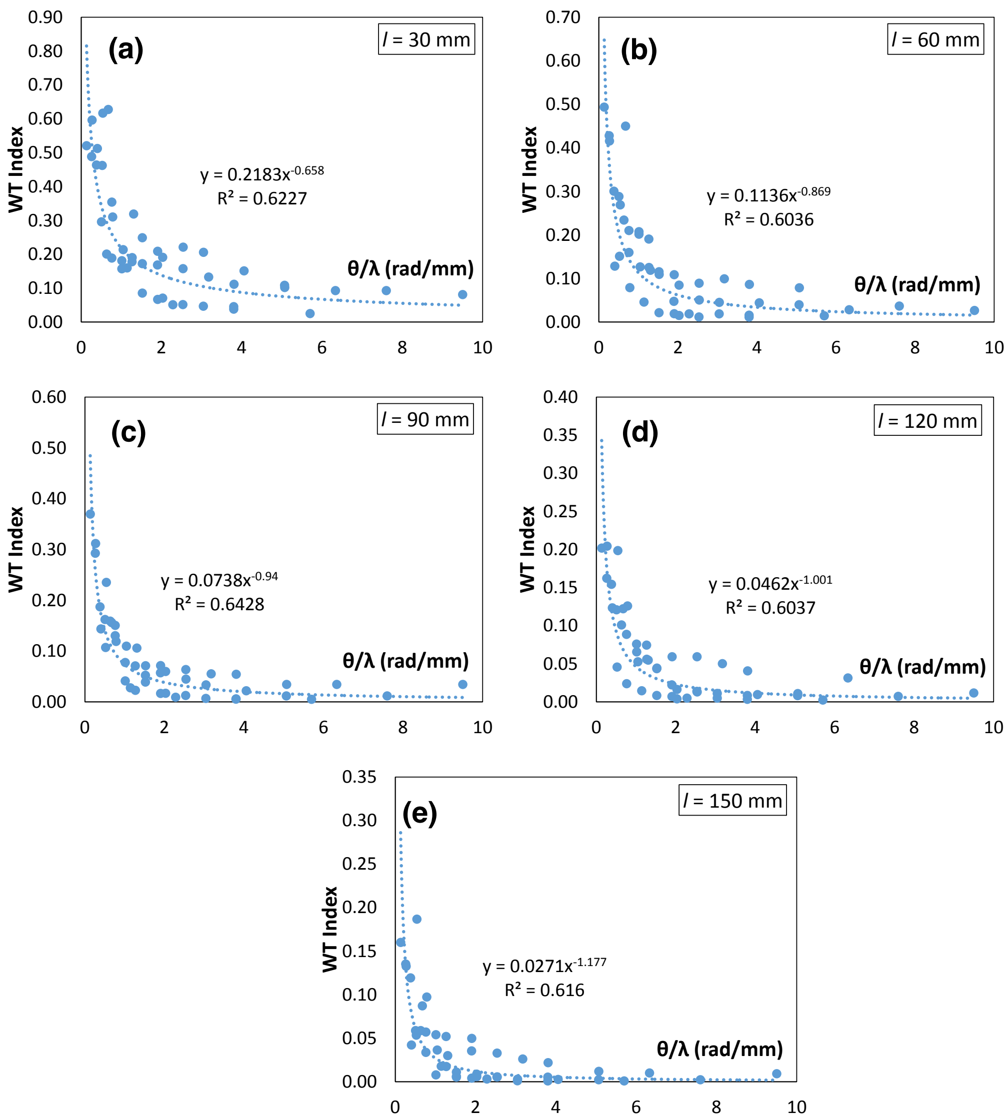


**Figure 10.** WT index versus $\theta/\lambda$ for steel reinforced concrete model with (a) 30 mm notch length cases, (b) 60 mm notch length cases, (c) 90 mm notch length cases, (d) 120 mm notch length cases and (e) 150 mm notch length cases

**Figure**

**Click here to download Figure: Figure 11.docx**

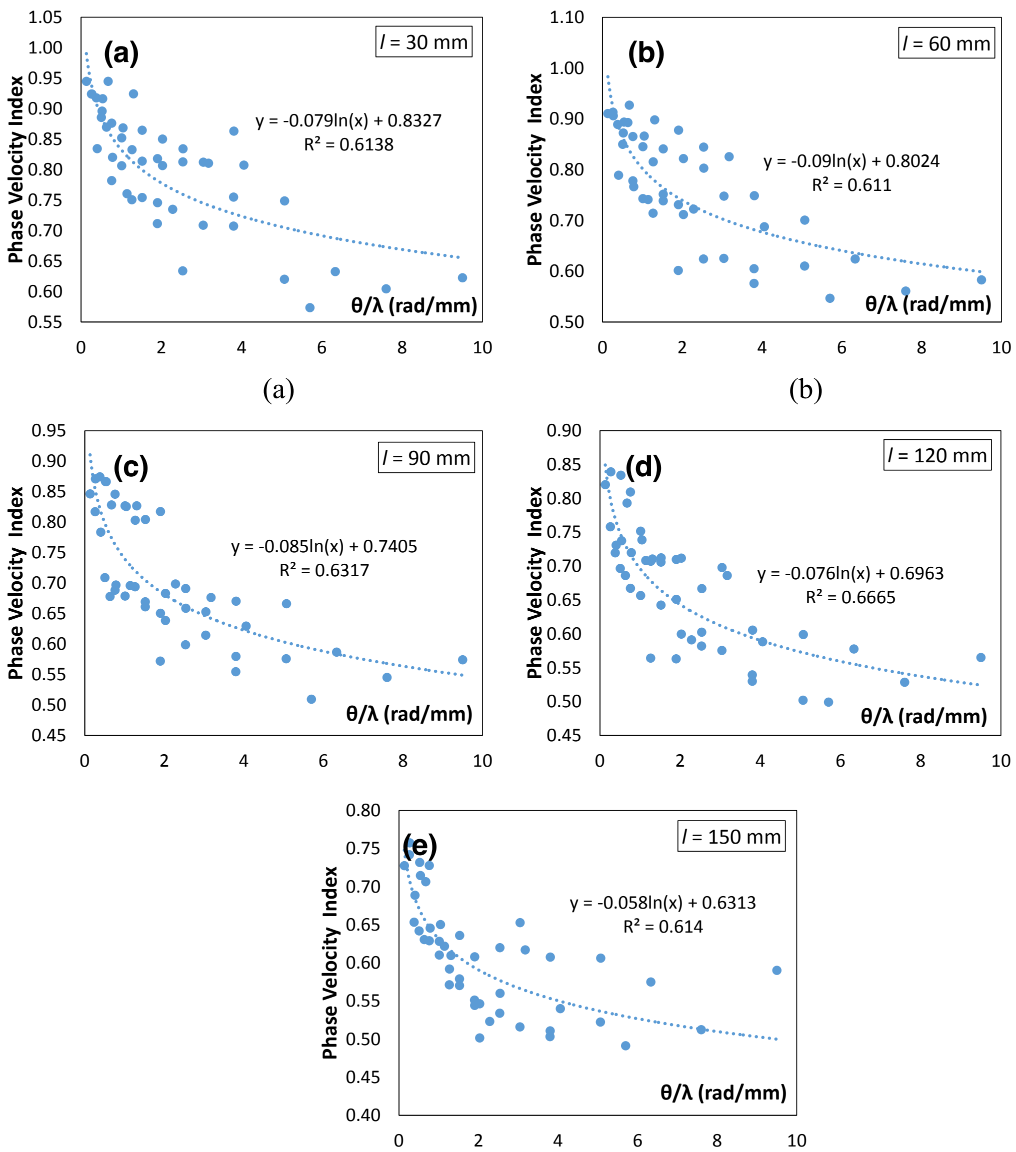


**Figure 11.** Phase velocity index versus $\theta/\lambda$ for steel reinforced concrete model with (a) 30 mm notch length cases, (b) 60 mm notch length cases, (c) 90 mm notch length cases, (d) 120 mm notch length cases and (e) 150 mm notch length cases

Figure
Click here to download Figure: Figure 12.docx

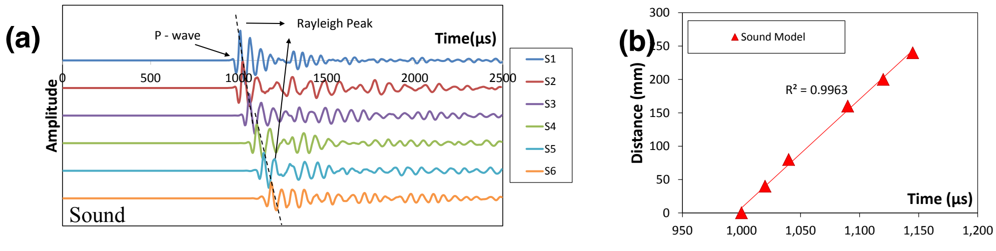


**Figure 12.** Experimental waveforms collected for (a) sound concrete specimen and (b) their corresponding R-waves propagation distance against arrival time. Excitations were done by 19 mm steel ball impact.

**Figure**
**Click here to download Figure: Figure 13.docx**

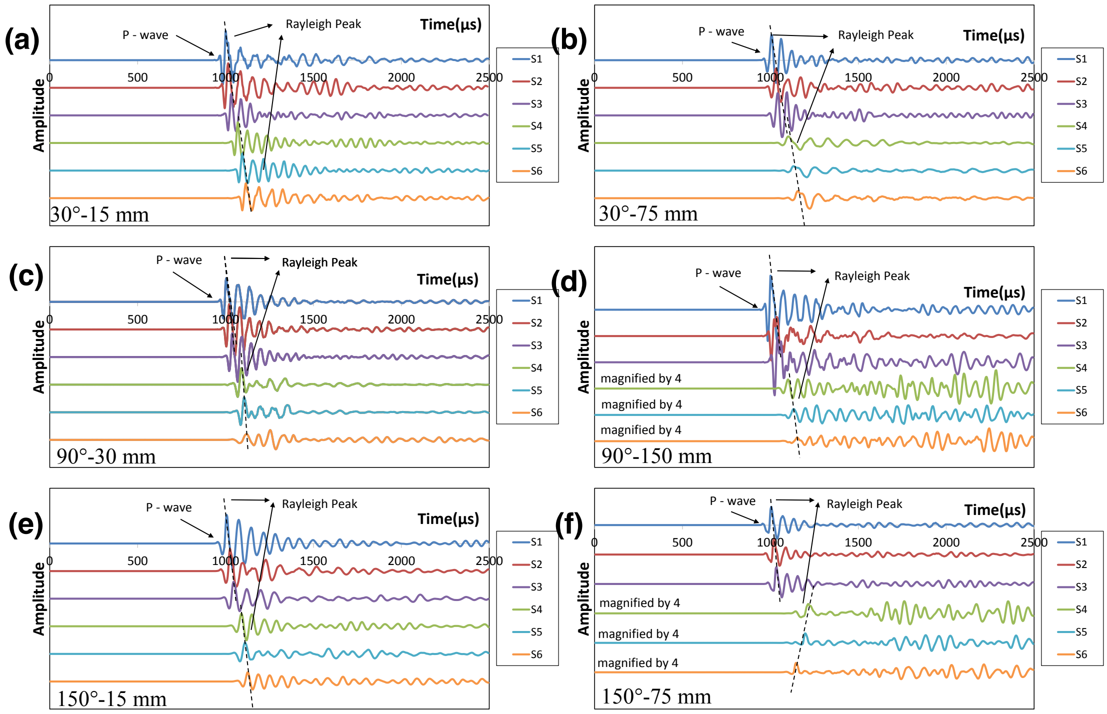


**Figure 13.** Experimental waveforms collected for (a) 15 mm 30° inclined notch, (b) 75 mm 30° inclined notch, (c) 30 mm 90° vertical notch, (d) 150 mm 90° vertical notch, (e) 15 mm 150° inclined notch and (f) 75 mm 150° inclined notch. Excitations were done by 19 mm steel ball impact.

**Figure**

**Click here to download Figure: Figure 14.docx**

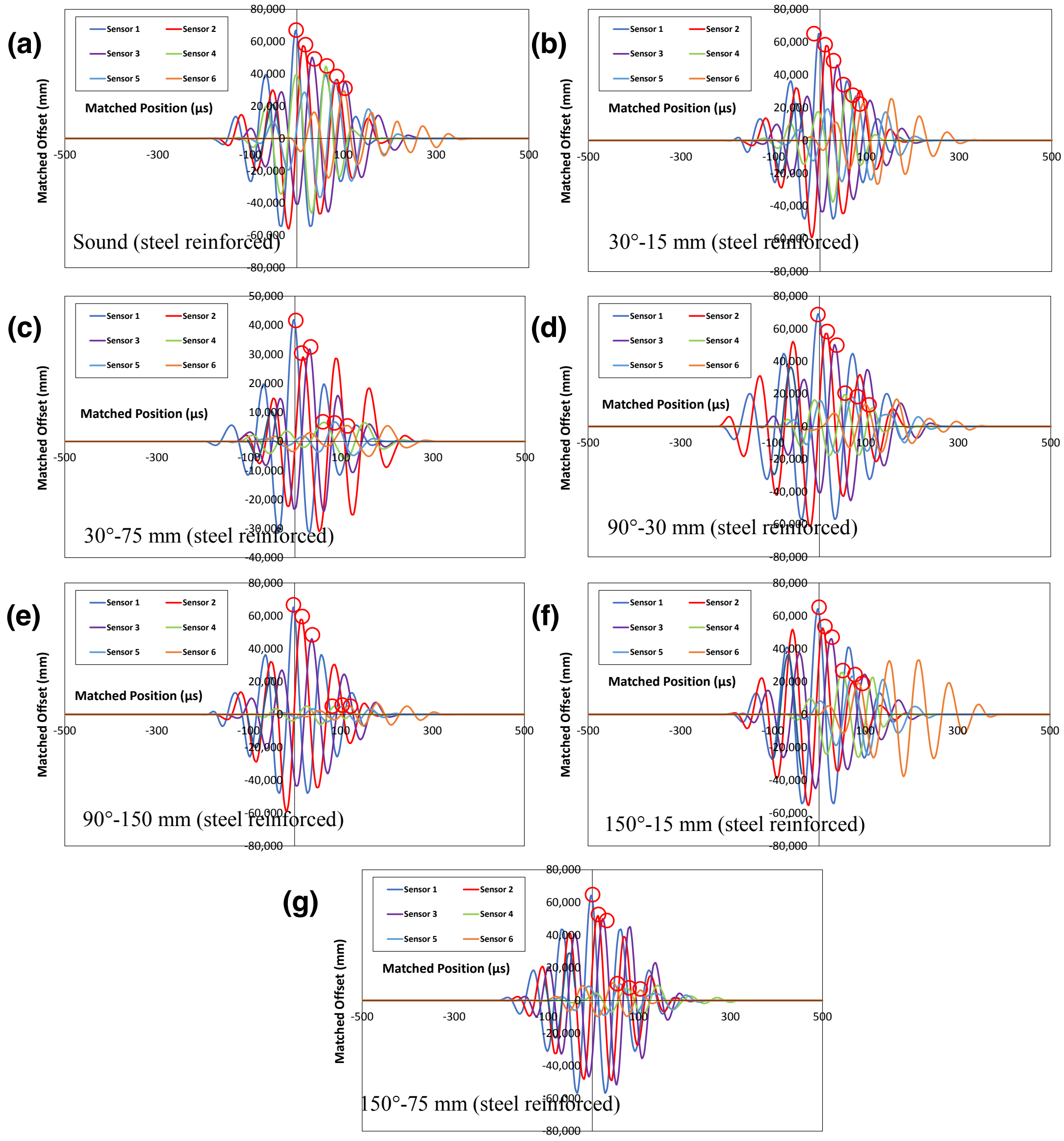


**Figure 14.** Processed experimental waveforms and the respective final R-wave peak matched positions based on MFCE method for (a) sound, (b) 15 mm 30° inclined notch, (c) 75 mm 30° inclined notch, (d) 30 mm 90° vertical notch, (e) 150 mm 90° vertical notch, (f) 15 mm 150° inclined notch and (g) 75 mm 150° inclined notch. Excitations were done by 19 mm steel ball impact.

**Figure**

Click here to download Figure: Figure 15.docx

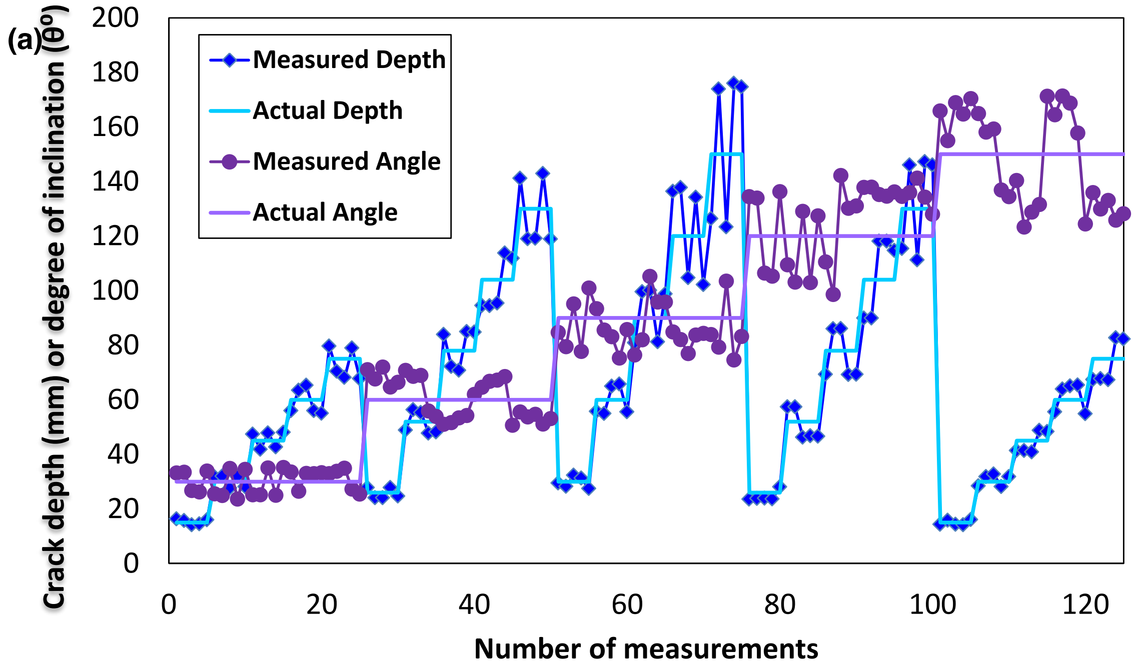


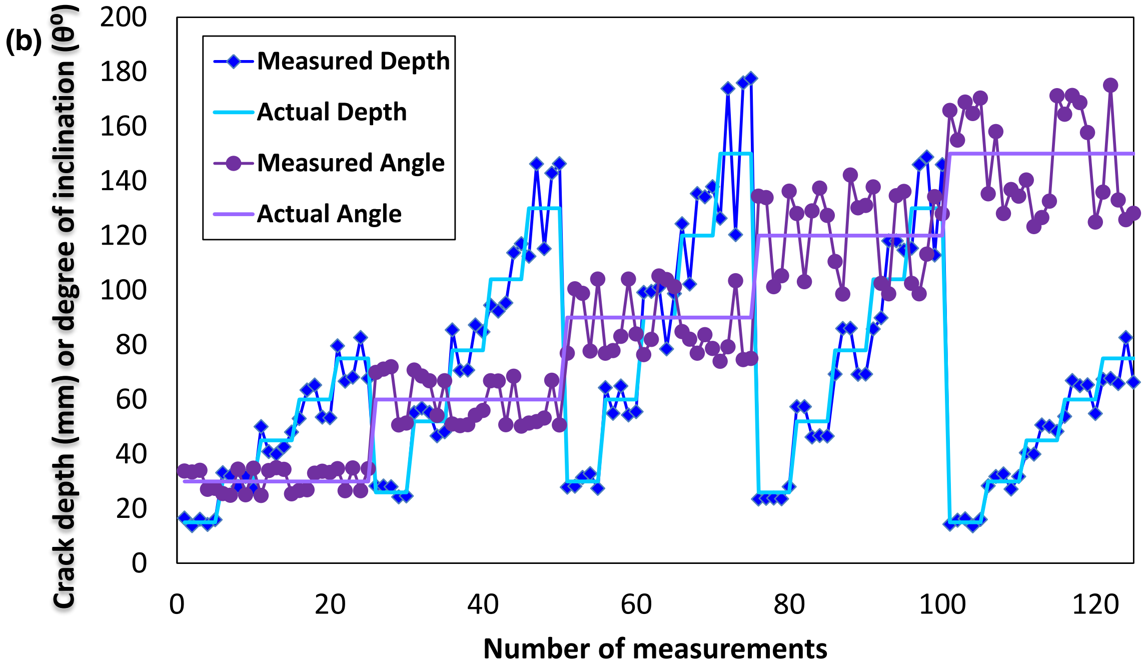

**Figure 15.** Surface notch depth and degree of inclination estimations based on (a) WT index (b) phase velocity index.